THE UNIVERSITY OF MANITOBA

THE EFFECTS OF ELASTIC STOPS AND INELASTIC RESTRAINERS ON VIBRATING BEAM-LIKE STRUCTURES

BY

ALI FATHI

A DISSERTATION SUBMITTED TO THE FACULTY OF GRADUATE STUDIES OF THE UNNIVERSITY OF MANITOBA IN PARTIAL FULFILLMENT OF THE REQUIREMENTS OF THE DEGREE OF

DOCTOR OF PHILOSOPHY

DEPARTMENT OF MECHANICAL ENGINEERING

WINNIPEG, MANITOBA

February, 1985

THE EFFECTS OF ELASTIC STOPS AND INELASTIC RESTRAINERS ON VIBRATING BEAM-LIKE STRUCTURES

BY

ALI MOHAMED FATHI

A thesis submitted to the Faculty of Graduate Studies of the University of Manitoba in partial fulfillment of the requirements of the degree of

DOCTOR OF PHILOSOPHY

THE EFFECTS OF ELASTIC STOPS AND INELASTIC RESTRAINERS ON VIBRATING BEAM-LIKE STRUCTURES

TABLE OF CONTENTS

ABSTRACT

An approximate technique is developed to determine the flexural response typical of many practical vibroimpact applications. The technique is shown to significantly reduce computational effort whilst largely preserving accuracy. However, accuracy can be improved by selectively combining the approximate technique with a purely numerical approach to enhance the details of important contact forces. The ensuing computational requirements, although increased somewhat, are still sufficiently small to permit the use of a desk-top computer. Problems associated with a user-friendly presentation of the dynamic interactions between a structure and stop are outlined. The possibility of fine detail associated with chatter gaining prominence may be assessed from a priori information by employing a newly developed energy criterion. A very computationally economical approach is formulated later to predict the maximum impact forces which are important from a design point of view. The main novelty in the latter approach lies in the effective use of non-dimensional vibroimpact parameters obtained from the equations of motion. These parameters allow subsequent results to be merely extrapolated from any one previously computed case. Then

computational savings are potentially tremendous in design situations where many computer runs are usually needed.

A comprehensive study is also conducted to complement previous experimental work and assess the effectiveness of inelastic restrainers. The theoretical model is based upon a finite element approach and dynamic condensation is introduced to reduce computational effort. An example is presented wherein a two-dimensional U-frame is subjected to the TAFT S69E earthquake. Results tend to show that yielding materials are ineffective absorbers of seismic energy.

ACKNOWLEDGEMENT

Thanks are due to Dr N. Popplewell (advisor), Dr A. Shah and Dr K. McLachlan. I would also like to express my appreciation to Dr R. J. Rogers (external examiner), not only for reading the thesis but also for attending the oral examination.

The valuable suggestions and advices of Dr D. Trim are greatly appreciated. I would also like to thank Mr D. R. Young (the computer wizard).

Thanks are also due to the University of Manitoba for providing me with a graduate scholarship and a teaching assistantship. Financial support was also received from the National Science and Engineering Research Council of Canada under the research grant of Dr N. Popplewell.

The moral support I received from all my friends was extremely helpful.

Very special thanks are expressed to Chris and Jim who introduced a new meaning to the word "friendship".

Finally I am greatful to my one and only love "Nagla" whose enormous sacrifices and continuous encouragement have significantly contributed to the completion of this thesis.

LIST OF FIGURES

LIST OF TABLES

CHAPTER 1
INTRODUCTION

A vibroimpact stop or snubber is essentially an elastic body which intermittently limits the displacement of an excessively vibrating structure. A typical situation is illustrated in general terms in Figure 1. The beam shown may have different boundary conditions but, more importantly, it vibrates so greatly transversely that collisions occur occasionally against the fixed stop. This rather simplified situation illustrates the basic behaviour of heat exchanger tubes in a turbulent fluid and power plant piping systems under a seismic load. The stop comes into play in the latter situation only for severe seismic disturbances. Then large excursions are restricted but high impact stresses are unavoidably produced which may lead to fretting wear of the contacting surfaces. Fretting will be dictated presumably by the frequency and intensity of impacts. Impact parameters will depend, in turn, upon the location, clearance and relative stiffness of the snubbers.

A velocity discontinuity is created at an impact [1] so that the principle of superposition does not hold globally. This principle, however, may be applied between any two successive contacts and during contacts providing

the structure and snubber separately obey Hooke's law [2]. Even so, presently available modal analysers, which are based on the precept of universal linearity, cannot easily handle colliding structures. Consequently, although vibroimpacts have been studied analytically [3] and numerically [1,4,5-8], complementary experimental data is much scarcer.

The most complicated structural model considered has been a beam moving transversely and colliding intermittently with an off-set, usually purely elastic spring. Although the stop was idealized as a spring and a dash pot in reference [7], the damping force was found negligible compared to the spring force. An elementary Bernoulli-Euler beam theory, appropriate to small deflections, has been mostly used and the probable plastic zone around a contact point has been neglected. Resulting theoretical and available experimental data correlated reasonably for clearances less than an appropriate beam's thickness. Rogers [1] extended Elliott's work [9] to obtain equations of motion by using a finite element formulation for the beam. A modal superposition approach was employed to numerically solve these equations. The finite element displacements were expressed in terms of the mode shapes and modal

amplitudes. Consequently, the number of resulting equations did not correspond to the degrees of freedom but rather to the number of modes which achieve solution convergence.

Lo [4] used a somewhat similar approach but treated the beam as a system having continuously distributed parameters. Hence, the beam's motion was described by a partial differential equation which has an analytical solution for non-contact periods where the system is linear. The Duhamel integral was evaluated numerically during a contact to calculate the response to the impact load which was treated as a series of impulses. To make the modal superposition approach feasible, both Rogers [1] and Lo [4] judiciously selected the number of modes employed in the solution. Quite often in practice, however, rapidly changing intermittent contact "*chatter*" may occur. In such cases, a severe discarding of higher frequency modes significantly eliminates the finer detail of the *chatter*.

Lo [4] was interested primarily in the performance of electromechanical relays and, hence, considered only free or no external load vibroimpact cases. Rogers [1], on the other hand, considered vibroimpact systems excited

externally by a sinusoidal point load in order to study the detrimental effect of flow induced vibrations in heat exchanger tubes. To determine the dynamic response of structural systems with clearances, Mariamy et al [3] concentrated on models with harmonic base excitations. An analytical steady-state solution was obtained [3] on the basis that only one impact occurs per excitation cycle and that the system's displacement and velocity are continuous throughout contact and non-contact periods. However, *chatter* can occur in some vibroimpact cases [4] and the continuity condition for the velocity is not always satisfied [1]. Therefore, besides neglecting the practically important transient response, the solution is not general.

The vibroimpact beam system detailed in reference [4] will be used in the present work for convenience. However, numerical illustrations will indicate that even this relatively simple beam example requires extensive computations even with fairly efficient algorithms. Free vibrations will be considered initially because the ensuing relatively simple problem can provide a first step towards more general vibroimpact situations. An energy criterion will be suggested by which the possibility of *chatter* may be predicted from a priori

information. A forced vibroimpact problem in which the external excitation is a sinusoidal point load will be considered separately. An approximate technique combining analytical and numerical procedures will be developed to determine the flexural response of a vibroimpacting beam. The approach significantly reduces computational effort yet largely preserves accuracy. Problems associated with a user-friendly presentation of the dynamic interactions between a structure and stop will be outlined.

Unlike linear systems, straightforward extrapolation from a specific vibroimpact case seems impossible. Therefore, an optimum design is obtained usually by selecting the "best" of several cases each of which requires a separate analysis. Unfortunately, the vibroimpact analysis is based mostly upon "brute force" numerical procedures where computations can be excessive. Therefore, a computationally economical approach will be developed to predict the practically important impact stresses. The main novelty in the approach lies in the effective use of a set of non-dimensional vibroimpact parameters developed from the equations of motion.

THEORY

1.2.a Approximate technique for determining the flexural response of a beam impacting a stop:

The basic theory will be limited to flexurally vibrating members having a large span to depth ratio for which Euler's elementary theory is applicable [10]. In practice, a motion limiting stop is usually lighter and much stiffer than the vibrating member [1]. Consequently, its fundamental natural frequency will be greater than the largest natural frequency effectively contributing to the dynamic response of the vibrating structure. Therefore, the contact force is dictated by the stiffness of the stop whose inertia can be neglected. This assumption is implemented by idealizing the stop as a massless spring. To be consistent with previous references [1,3-4,7-9,11-13], the vibrating structure is idealized as a beam with linear material properties. Neglecting shear deformations and rotational accelerations, the flexural deflection of the beam, $y(x,t)$, may be described by Euler's elementary theory of bending as

$$EI \frac{\partial^4 y}{\partial x^4} + C \frac{\partial y}{\partial t} + \rho A \frac{\partial^2 y}{\partial t^2} + N(t)\delta(x-b) = F(x,t) \quad . \quad (1)$$

It has been assumed in equation (1) that the beam is uniform and homogeneous with a constant flexural rigidity, EI, and a mass per unit length, ρA. A viscous damping coefficient, C, has also been presumed. The time varying external load, F(x,t), is generally a function of both the time, t, and distance, x, from the left end of the beam. Furthermore, the term $N(t)\delta(x-b)$ in equation (1), where δ is the Dirac delta function, describes the force exerted on the beam when it contacts the non-dissipative stop located at x=b. The Normal Mode solution of equation (1) may be written as [14]

$$y(x,t) = \left[\sum_{n=1}^{\infty} \phi_n(x) q_n(t) + \sum_{n=1}^{\infty} \frac{\phi_n(x)\phi_n(b)}{m\omega_{nd}} \int_0^t e^{-\zeta_n \omega_n (t-\tau)} N(t) \sin \omega_{nd}(t-\tau) d\tau \right] \quad (2a)$$

where $$\omega_{nd} = \omega_n \left(1 - \zeta_n^2 \right)^{1/2} . \quad (2b)$$

Subscript n designates the nth beam mode with shape $\phi_n(x)$ and critical damping ratio ζ_n at circular frequency ω_n. The $q_n(t)$ is the normal coordinate corresponding to $\phi_n(x)$ and m is the total mass of the beam. Details of

$\phi_n(x)$ and ω_n have been given by Bishop and Johnson [15]. An inspection of Figure 1 indicates that the beam's displacement at the point of contact is simply the algebraic sum of the clearance†, h, and the deflection of the beam during a collision. The latter movement can be obtained from Newton's law as $-N(t)/k$, where k is the linear stiffness of the stop, so that

$$y(b,t) = h - \frac{N(t)}{k} \tag{3}$$

during contact. Combining equation (3) with equation (2), evaluated at x=b, produces

$$h - \frac{N(t)}{k} = \left\{ \sum_{n=1}^{\infty} \phi_n(b) q_n(t) + \sum_{n=1}^{\infty} \frac{\phi_n^2(b)}{m\omega_{nd}} \int_0^t e^{-\zeta_n \omega_n (t-\tau)} N(t) \sin \omega_{nd}(t-\tau)\, d\tau \right. \tag{4}$$

Equation (4) can be solved for the unknown contact force, N(t), by using the small time increment technique [5].

---

† The clearance is defined as the distance measured from the tip of the undeflected spring to the static equilibrium position of the beam alone.

Alternatively, the approximation of N(t) by an appropriate analytical expression leads to an algebraic form of equation (4) which can be generally evaluated with much less computational effort. Having solved equation (4), equation (2) can then be used to determine the beam's displacement in the interval before the next collision. The subsequent alternate use of equation (4) and (2) leads to the complete history of the beam's deflection. Other variables of interest, like the bending moment and the shear force, may be found conventionally from the deflection [6].

The contact force may be treated as a sequence of impulses in the numerical evaluation of equation (4). Consequently, the continuous force-time curve is broken into increments (with respect to the time scale) as illustrated in Figure 2. Each increment corresponds to a typical impulse of the form $N(\tau)\Delta t$. The complete response to the contact force can be calculated by summing all the individual responses produced by each impulse. Thus, the discrete form of equation (4) becomes

$$\left.\begin{aligned}&\sum_{n=1}^{\infty} \phi_n(b) q_n(t) \; + \\ &\sum_{n=1}^{\infty} \frac{\phi_n^2(b)}{m\omega_{nd}} \sum_{t_*=t_0}^{t-\Delta t} e^{-\zeta_n \omega_n (t-t_*)} N(t_*+\Delta t)\; \Delta t \sin \omega_{nd}(t-t_*)\end{aligned}\right\} = h - \frac{N(t)}{k} \, . \qquad (5)$$

The second term on the left of the above equation represents the contribution of the contact force. Therefore, it comes into play only during a contact period typically represented by $t_0 \leq t \leq t_f$. Equation (5) may be solved recursively by separately setting t equal to $t_1, t_2, \ldots . t_f$ to sequentially determine $N(t_1), N(t_2), \ldots$ which approximate the complete history of the contact force as in Figure 2. The equation (5) typically becomes

$$N(t_i) = \frac{h - \sum_{n=1}^{\infty} \phi_n(b) q_n(t_i) - \sum_{n=1}^{\infty} P_i \frac{\phi_n^2(b)}{m\omega_{nd}} \sum_{t_j=t_0}^{t_i-2\Delta t} e^{-\zeta_n \omega_n (t_i - t_j)} N(t_j+\Delta t)\, \Delta t \sin \omega_{nd}(t_i - t_j)}{\frac{1}{k} + \sum_{n=1}^{\infty} \frac{\phi_n^2(b)}{m\omega_{nd}} e^{-\zeta_n \omega_n \Delta t} \Delta t \sin \omega_{nd} \Delta t} \qquad i = 1,2,3...$$

where

$$P_i = \begin{cases} 0 & i = 1 \\ 1 & i > 1 \end{cases} . \qquad (6)$$

For an accurate history Δt must be, at most, half the period corresponding to the highest structural frequency (or lowest period) excited by the impact [4]. However, actual values are usually taken somewhat lower. For example, Lo [4] used Δt equal to 1/6th of the lowest period of the excited modes. Unfortunately, a structure normally responds in a large number of modes at an impact with relatively stiff stops [4]. Typically nine and fifteen modes were excited in the examples reported in reference [1] and [4]. Therefore, Δt must be chosen very small which significantly increases the number of increments defining the contact force. Consequently, the

successive evaluation of equation (6) becomes uneconomical computationally.

An alternative approach is to approximate the contact force, N(t), by a continuous function over an entire contact. To obtain an approximate form, recall that the Normal Mode Technique essentially reduces a structure to a set of independent oscillators. Hence, the form of N(t) can be visualized from the example shown in Figure 3. This figure illustrates the forced vibration of a single oscillator colliding intermittently with a resilient stop. A detailed analysis of the vibration of this system is given in Appendix A1 under those resonant conditions where stops are primarily used. The analysis shows that, for relatively stiff stops (i.e much stiffer than the vibrating structure), the contact force N(t) is half sinusoidal in form. This form can be expressed mathematically as

$$N(t) = A \sin ft \qquad 0 \leq ft \leq \pi \qquad (7)$$

with the first instant of an impact taken as the temporal origin. The A and f are the magnitude and frequency of the half sinusoid, respectively. By analogy, approximation

(7) is likely to be valid for continuous vibroimpact systems with relatively stiff stops. Equation (4) and (7) can then be combined and the integral evaluated to produce

$$\sum_{n=1}^{\infty} \phi_n(b) q_n(t) + \sum_{n=1}^{\infty} \frac{\phi_n^2(b)\ A}{m\omega_{nd}\ \ 2} e^{-\zeta_n\omega_n t} D(t) = h - \frac{A \sin ft}{k} \quad (8a)$$

where

$$D(t) = \begin{cases} \zeta_n\omega_n e^{\zeta_n\omega_n t}\cos ft\ (C_1-C_2) + e^{\zeta_n\omega_n t}\sin ft\ (C_3-C_4) \\ + \zeta_n\omega_n \cos \omega_{nd}t\ (C_2-C_1) + \sin \omega_{nd}t\ (C_3+C_4) \end{cases} \quad (8b)$$

with

$$C_1 = \left[\zeta_n^2\omega_n^2 + (f+\omega_{nd})^2 \right]^{-1} ,$$

$$C_2 = \left[\zeta_n^2\omega_n^2 + (f-\omega_{nd})^2 \right]^{-1} , \quad (8c)$$

$$C_3 = \frac{f + \omega_{nd}}{\left[\zeta_n^2\omega_n^2 + (f+\omega_{nd})^2 \right]} ,$$

and

$$C_4 = \frac{f - \omega_{nd}}{\left[\zeta_n^2\omega_n^2 + (f-\omega_{nd})^2 \right]} .$$

The A and f are the only two unknowns in equation (8a). Two simultaneous equations will be produced if this equation is evaluated at two distinct values of ft between 0 and π. Elimination of A between the equations obtained for ft equal π/2 and π, for example, yields the following transcendental equation in f

$$\frac{h - \sum_{n=1}^{\infty} \phi_n(b) q_n\left(\frac{\pi}{2f}\right)}{\sum_{n=1}^{\infty} \frac{\phi_n^2(b)}{2m\omega_{nd}} e^{-\zeta_n \omega_n \frac{\pi}{2f}} D\left(\frac{\pi}{2f}\right) + \frac{1}{k}} = \frac{h - \sum_{n=1}^{\infty} \phi_n(b) q_n\left(\frac{\pi}{f}\right)}{\sum_{n=1}^{\infty} \frac{\phi_n^2(b)}{2m\omega_{nd}} e^{-\zeta_n \omega_n \frac{\pi}{f}} D\left(\frac{\pi}{f}\right)} . \qquad (9)$$

If the stop is relatively stiff then the contact duration is expected to be smaller than the period of the vibrating structure's fundamental mode and essentially unaffected by the number of modes excited. Equation (9) can then be reduced to the following simpler form;

$$\frac{h - \phi_1(b) q_1\left(\frac{\pi}{2f}\right)}{\frac{\phi_1^2(b)}{m} \frac{\pi}{2f^2} + \frac{1}{k}} = \frac{h - \phi_1(b) q_1\left(\frac{\pi}{f}\right)}{\frac{\phi_1^2(b)}{m} \frac{\pi}{f^2}} . \qquad (10a)$$

for $$\pi/f << 2\pi/\omega_1 . \qquad (10b)$$

Equation (10a) can now be solved straightforwardly for f which can then be substituted in equation (8a) to determine A.

1.2.b Economical approach for predicting impact forces and stresses :

Equations pertinent to the vibroimpacting cantilevered beam illustrated in Figure 4 will be expressed non-dimensionally in this section. This procedure gives a physical insight into the interplay between various vibroimpact variables. The resulting set of non-dimensional groups can also be used to generalize the impact stresses of any given but invariant structure-stop configuration.

The motion of the vibroimpact system shown in Figure 4 is described by equation (1) with F(x,t) set to zero during a contact. When damping is neglected, the Normal Mode Method [14] yields the solution of equation (1) as

$$y(x,t) = \sum_{n=1}^{\infty} \phi_n(x) q_n(t) + \sum_{n=1}^{\infty} \frac{\phi_n(x)\phi_n(b)}{m\omega_n} \int_0^t N(\tau) \sin \omega_n(t-\tau) d\tau. \qquad (11)$$

The maximum bending stress at any section along the beam is given by [2]

$$\sigma(x,t) = \frac{M_z(x,t)}{Z} \qquad (12)$$

where Z is the section modulus and $M_z(x,t)$ is the corresponding bending moment. The Bernoulli-Euler elementary bending theory relates the bending moment to the curvature, $\partial^2 y(x,t)/\partial x^2$, as

$$M_z(x,t) = EI \frac{\partial^2 y(x,t)}{\partial x^2} \tag{13}$$

where E is Young's modulus and I is the moment of inertia of the cross section at position x and instant t. Combining equations (11),(12) and (13) gives the bending stress as

$$\sigma(x,t) = \frac{EI}{Z} \sum_{n=1}^{\infty} \frac{d^2 \phi_n(x)}{dx^2} \left[q_n(t) + \frac{\phi_n(b)}{m\omega_n} \int_0^t N(\tau) \sin \omega_n(t-\tau)\, d\tau \right] . \tag{14}$$

To obtain the contact force N(t), equations (3) and (11) are combined for x=b to give the integral equation

$$\sum_{n=1}^{\infty} \phi_n(b) q_n(t) + \sum_{n=1}^{\infty} \frac{\phi_n^2(b)}{m\omega_n} \int_0^t N(\tau) \sin \omega_n(t-\tau) d\tau = h - \frac{N(t)}{k} \qquad (15)$$

which can be solved numerically. The numerical process must be repeated for each combination of vibroimpact parameters like h,k, etc.

Alternatively, equation (15) can be manipulated such that direct extrapolation from specific data becomes possible. Because an impact is typically very short, the contact force, N(t), can be often reasonably approximated by a single impulse of duration ΔT and magnitude $M\Delta T$ as suggested in Figure 5. Incorporating this approximation (i.e. $N(\tau) = M\Delta T\, \delta(\tau - t_o)$) into equation (15) gives an equation which can be solved for M, namely

$$M = \frac{h - \sum_{n=1}^{\infty} \phi_n(b)\, q_n(t)}{\frac{1}{k} + \sum_{n=1}^{\infty} \frac{\phi_n^2(b)}{m\omega_n} \Delta T \sin \omega_n(t-t_o)} \qquad (16)$$

Here t_o is the instant at which contact first occurs. Care must be exercised before attempting to use equation (16). The value of M is accurate only when ΔT happens to be less than the period of the highest beam mode excited at impact. If this is not the case, then a loss of accuracy can be expected. However, the ratio between the actual value of M and the one calculated by using equation (16) will be constant for an invariant configuration. Therefore, equation (16) can then be used safely to provide relative rather than absolute values.

Terms in equation (16) can now be grouped into dimensionless parameters. This procedure can be done in various ways - some more advantageous than others. For example, normalization of N(t) with respect to kh introduces singularities at h equals zero when there is no external load. Similarly, a singularity occurs if the modal displacements, $q_n(t)$, are normalized with respect to y(b,0) in a forced vibroimpact case where the beam is at rest initially. In the present work, equation (16) is manipulated into a dimensionless form appropriate to cases with no external loads. The product $m\omega_n$ is replaced first by $(\lambda_n \ell)^4 EI/\ell^3/\omega_n$ because [15]

$$\omega_n^2 = \left(\frac{\lambda_n \ell}{\ell}\right)^4 \frac{EI}{\rho A} \quad . \qquad (17)$$

Next, the initial displacement of the beam's potential point of contact, y(b,0), is added and subtracted from the numerator on the right of equation (16). Finally, equation (16) is divided by the product k[h-y(b,0)]. These operations produce

$$\frac{1}{N^*} = \frac{1 + \frac{1}{h^*}\left[1 - \sum_{n=1}^{\infty} \phi_n(b) \frac{q_n(t)}{y(b,0)}\right]}{1 + \sum_{n=1}^{\infty} \frac{\phi_n^2(b)}{(\lambda_n \ell)^4} K^* (\omega_n \Delta T) \sin \omega_n (t-t_o)} \qquad (18)$$

where

$N^* = \frac{k\,[\,h-y(b,0)\,]}{M}$ is the relative contact force;

$K^* = \frac{k\ell^3}{EI}$ corresponds to the relative stiffness; and

$h^* = \frac{h - y(b,0)}{y(b,0)}$ is the relative clearance.

To illustrate the usefulness of equation (18) in design, consider the cantilevered beam of Figure 4 with its free end deflected initially to $y(\ell,0)$. Upon release, the beam freely travels downwards. When it encounters the stop "*chattering*" or rapidly changing intermittent contacts could take place [4]. An energy criterion for predicting the possibility of *chatter* is developed in Appendix A2. When the beam eventually ceases *chattering* and resumes its initial deflected position (because no damping is present), the cycle will repeat itself [4]. For safety, vibroimpact designs are based upon maximum contact forces which always occur in this particular example when the beam is deflected fully before an impact, i.e. when the beam conditions are:

$$y(x,t_1) = \frac{y(\ell,0)}{2\ell^3}\,(3x^2\ell - x^3)$$

and (19)

$$\dot{y}(x,t_1) = 0 \quad .$$

Here t_1 is a representative temporal origin at the beam fully deflected position. In fact, the conditions can be considered to be "initial" conditions for the beam's

subsequent period of no-contact vibration. Consequently, the t_1 can be shifted for each period between consecutive impacts to zero. By letting t equal the particular value of $(t_o+\Delta T)$, terms in equation (18) are no longer time dependent which is more useful for the purpose of design. Equation (18) then becomes

$$\frac{1}{N^*} = \frac{1 + \frac{1}{h^*}\left[1 - \sum_{n=1}^{\infty} \phi_n(b)\ \frac{q_n(t_o+\Delta T)}{y(b,0)}\right]}{1 + \sum_{n=1}^{\infty} \frac{\phi_n^2(b)}{(\lambda_n \ell)^4} K^*\ (\omega_n \Delta T)\ \sin\ \omega_n(\Delta T)} \quad . \qquad (20)$$

If K* is kept constant, for example, then the N* which correspond to different values of h* can be extrapolated from the exact data of any single known case† by using

$$N^* = N^*\Big|_{\substack{\text{known}\\ \text{case}}} \frac{1 + \frac{1}{h^*}\left[1 - \sum_{n=1}^{\infty} \phi_n(b)\ \frac{q_n(t_o+\Delta T)}{y(b,0)}\right]_{\substack{\text{known}\\ \text{case}}}}{1 + \frac{1}{h^*}\left[1 - \sum_{n=1}^{\infty} \phi_n(b)\ \frac{q_n(t_o+\Delta T)}{y(b,0)}\right]},$$

K* constant . (21)

Similarly, the effect of changing K* while keeping the

---

† A subscripted known case is one where values have been previously determined numerically from equation (15).

non-dimensional clearance parameter h* constant can be examined through

$$N^* = N^*\Big|_{\substack{\text{known}\\ \text{case}}} \frac{1 + K^* \sum_{n=1}^{\infty} \frac{\phi_n^2(b)}{(\lambda_n \ell)^4} \omega_n(\Delta T)' \sin \omega_n(\Delta T)'}{1 + K^*\Big|_{\substack{\text{known}\\ \text{case}}} \sum_{n=1}^{\infty} \frac{\phi_n^2(b)}{(\lambda_n \ell)^4} \omega_n(\Delta T) \sin \omega_n(\Delta T)},$$

h* constant . (22a)

Rogers [1] has shown that the contact duration ΔT is inversely proportional to the square root of K^*. Therefore,

$$(\Delta T)' = \Delta T \left[\frac{K^*\Big|_{\substack{\text{known}\\ \text{case}}}}{K^*} \right]^{1/2}. \qquad (22b)$$

Values determined from equation (21) or (22a) for N^* constitute a dimensionless group which can provide the magnitude of the contact force. The latter can then be substituted in equation (14) to straightforwardly calculate the corresponding bending stress, $\sigma(x,t)$.

RESULTS AND DISCUSSION

For convenience, the theories of Section 1.2.a and 1.2.b are called the "approximate" and "economical" techniques, respectively. Their inherent assumptions and relative merits were assessed by employing the transversely vibroimpacting beams detailed previously by Lo [4] and Rogers [1]. The material properties and related constants pertaining to these two references are given in Table 1. The assessment essentially compares results with "reference" solutions obtained by numerically solving equations (2) and (4). The numerical solutions were evaluated pragmatically by using a finite number of terms corresponding to the normal modes actually excited by an impact rather than the infinite number demanded theoretically. In actuality nine and fifteen normal modes were used to determine the reference solutions for the examples considered in reference [1] and [4], respectively. Furthermore, the time increment of integration, Δt, was always chosen smaller than 1/10th of the lowest modal period of a beam. Consequently, reference solutions were found to be virtually exact. A further 30 % increase in the number of modes, for example, changed the amplitude of the practically important contact force by only about 1 %. Several illustrations of rapid collisions

or chatter were also considered to substantiate simple energy-based predictions of this behaviour. These illustrations were based upon the material properties given in reference [4].

Equation (2) and (4), derived in Section 1.2.a, were incorporated in a digital computer program. This program included an optional feature which enabled the equations to be evaluated either numerically or by employing approximation (7). The externally loaded vibroimpact case considered in reference [2] was used to test the accuracy of the approximate technique. The load was sinusoidal in time with an amplitude of 0.1 lb_f and a frequency corresponding to the undamped and unrestrained beam's fundamental natural frequency. Figure 6 shows the contact force, N(t), calculated numerically during the first contact interval by employing upto the nine modes associated with the reference solution. The force histories are quite symmetrical for three, five or seven normal modes and they peak sharply around the middle of the resulting period. The more accurate use of nine modes, on the other hand, produces an elongated "tail" after about 3.525×10^{-2} secs. It is also clear from Figure 6

that the peak force is affected similarly by the number of normal modes considered. The peak, for example, grows quite substantially by 25 % or so for each halving in the number of modes from the reference situation. Now the half-sine approximation (7) assumes symmetry so that its utilisation will be analogous to employing a small number of modes. This observation suggests that the approximate technique could provide a quick, computationally efficient overview of the vibrating beam's dynamics but that its use will probably not produce accurate details like *chatter*. However, the simple energy-based chatter criterion described in Appendix A2 might then be useful.

The validity of the most efficient outcome of the approximate technique, namely equation (10a), depends upon the assumption of a stiff stop or, equivalently, the appropriateness of inequality (10b). Now the reference contact duration ,π/f, in the previous example is approximately 0.37 msecs. It is significantly smaller, therefore, than the period, $2\pi/\omega_1$ or 23.7 msecs, corresponding to the fundamental mode of the vibrating structure. Consequently, inequality (10b) is valid in this particular instance. However, the approximate technique cannot provide even an overview if approximation

differences introduced at the first contact become overly exaggerated over time. Therefore, later reference and approximate histories are compared in Figure 7.

The first three contact forces are presented in the centre of Figure 7 whilst the displacement between impacts at the tip of the beam is displayed at the bottom. Solid and dotted lines correspond to the reference and approximate results, respectively. The solution of equation (10a) provided the approximate contact duration. The corresponding approximate magnitude was obtained from equation (8a) which was truncated (in an analogous fashion to the reference solution) after nine terms. Correlations between the reference and approximate contact forces given in Figure 7 are satisfactory initially but appear to somewhat deteriorate progressively with time. Therefore, small differences in the deflection and inertia conditions of the beam at the end of the first contact (which arise from the enforced symmetry of the half-sine approximation) seem to be exaggerated ultimately. On the other hand, the tip's displacement illustrates the overall good agreement for the beam's deflection. Therefore, a reasonable prediction of the temporal start of any impact should be expected from the approximate technique because

these instants are merely a function of the displacement of the beam's point of contact.

The accuracy of predicting late contact forces can be improved by combining the approximate and purely numerical approach of the reference solution. Figure 8d shows the history of the illustrative 11th contact force calculated by using the combined technique. Also included are the corresponding force histories from either the approximate or the reference solution alone. In the combined approach, the beam's conditions at the end of the tenth impact were determined first by employing the approximate technique. The good accuracy of these approximate conditions is demonstrated in Figure 8a, b and c by their agreement with the corresponding reference displacement, velocity and acceleration. The approximate conditions at the end of the tenth impact were then used to numerically calculate the details of the eleventh impact in a manner identical to that of the reference solution. As can be seen from Figure 8d, the joint technique provided a reasonably accurate force history. More importantly, a computational saving of two orders of magnitude was achieved. This substantial saving permitted the computer program to run in an interactive fashion on a readily available Hewlett-Packard 9845 desk-top

computer.

Typical results from a self-contained computer package are presented in Figure 9 and 10. The programmable keys listed in Figure 9, for instance, formed a simple and user-friendly means of activating fairly complex subroutines. Furthermore, the listing can be recalled at almost any time to refresh the user's memory. Subsequent technical information can be displayed in a "dynamic" (animated) or "static" (frozen) format. Animation provided an overview of the impacting system's dynamic behaviour. It also helped a user to select appropriate structural points and instants of particular interest for additional detailed presentations in the "static" mode. Static presentations consisted of more design orientated specifics like the histories of the velocity, shear stress, bending moment, etc. at a point of contact or even the particulars of a contact force itself.

An illustrative example of various time histories is presented in Figure 10 for a cantilevered beam colliding at its "free" tip with a fixed stop. The topmost static or frozen frame indicates the instant upto which the histories are given. Lower frames represent the corresponding displacement, velocity and acceleration

histories at the tip. A velocity discontinuity can be seen just before the end of the computer-drawn trace in the lower left frame. Hence, these histories are shown up to an instant just after release from the first impact. The tip was selected with the help of a blinking cursor. The cursor moved intermittently but steadily across the upper static display of the structure and a key was depressed whenever a point of interest was reached. After confirmation by an audible tone, this location was computed automatically from the known speed and number of preceeding intermittent movements and its coordinates were stored.

Two major problems were partially overcome in the animation procedure. When the stucture approached the stop, the time increment associated with the theory was decreased to better define the initial instant of impact and thereby improve computational accuracy. Straightforwardly plotting the corresponding deflections at these initial instants would give the artificial visual impression of a deceleration. On the other hand, the resulting "slow-motion" could be useful in more closely inspecting the nature of an impact. Only part of the generated information, conversely, is pertinent to a true real-time presentation. Consequently, the ratio of the two

algorithm time increments was made a constant integer, n, and "real-time" data was displayed only at every nth instant. Another major problem was related to the geometry of the constructed images. A structure was represented by line segments defined by the co-ordinates of their end nodes. Obviously, more segments will produce a finer structural representation. However, the drawing speed of the computer employed decreased exponentially with an increasing number of segments. In fact, a visually disruptive blank screen was found to occur invariably between consecutive frames of an animated display. A link-by-link erasing and immediate redrawing technique was adopted to somewhat disguise the blank periods. Furthermore, only the links with a moving node between consecutive frames were affected. If movements were so small to be virtually invisible, then a zoom feature enabled geometric details to be magnified.

Although the briefly described presentation of computer-generated information is useful, it is only one step towards a true Computer-Aided-Design capability. Correction of the problems arising from a previous analysis would presently need skilful manipulation of clearances, modification of stop stiffnesses or even the

insertion of additional stops,etc. by an experienced operator.

The validity of the energy criterion, outlined in Appendix A2, was checked for an undamped cantilevered beam colliding at its tip with a fixed elastic stop. The material properties were taken from reference [1]. Various response histories of this vibroimpact system are presented in Figure 11. The beam's total kinetic and strain energy histories are also displayed in the upper half of the figure . It is apparent from the regularity of both energies that the beam travels initially in its first mode until it impacts the stop- at which instant a discontinuity can be observed. The traces then become irregular with the total kinetic energy subsequently reaching a (non-zero) minimum. This irregularity suggests that beam modes higher than the fundamental are excited at the impact. The corresponding shape histories in the lower part of Figure 11 show that the beam's tip goes through a rapid succession of intermittent contacts with the stop between 10.7 and 13.2 msecs . Furthermore, the maximum vertical distance between the stop and the beam's tip during a period of no contact is small compared to the beam's initial deflection. Therefore, the beam clearly

chatters against the stop. Now it can also be observed from Figure 11 that the beam's total kinetic energy is greater than its corresponding strain energy immediately before the contact. This implies that condition (A2.4) is not only satisfied but also predicts this chatter. Further illustrations of the criterion are summarised by energy values prior to the first contact which correspond to the different clearances, h, presented in Table 2. The invariably larger kinetic than corresponding strain energies in Table 2 would predict chatter which, indeed, occurred in all these instances. Consequently, these examples reinforce the applicability of the energy criterion.

Elliott [9] suggested that reducing the stiffness of a beam by modifying its geometry will reduce the amplitude of chatter when it exists. It was shown previously that the dynamic behaviour of a vibroimpacting beam is a function of the relative stiffness K* or $EI/k\ell^3$. Therefore, decreasing the beam's stiffness, EI/ℓ^3, is equivalent to correspondingly increasing the stop's stiffness, k. Two values of K*, 2.18×10^4 and 3.34×10^4, were used to determine the displacement histories of Figure 12. Each history was normalized with respect to the maximum tip

displacement (which occurs for the beam alone) to facilitate a comparison. A 35% reduction in K^* by virtually doubling k, whilst keeping E,I and ℓ constant, leads to essentially identical histories and, hence, a very slight reduction in chatter. This implies that an appreciable reduction in chatter may require a mostly impractical substantial decrease in K^* . Another drawback of Elliott's suggestion is related to the impact force. It should be recalled that for the particular example associated with Figure 12, K^* was altered solely by changing the stop's stiffness, k. Now all the terms except K^* and $(\Delta T)'$ on the right side of equation (22a) pertain either to the known and invariant reference situation or to the behaviour of the beam alone. Consequently, only K^* and $(\Delta T)'$ will change with k in this instance. A rise in k will proportinately decrease K^* which, in turn, equation (22b) indicates will only somewhat increase $(\Delta T)'$. Therefore, the generally governing product $K^*(\Delta T)'$ in the numerator of equation (22a) will be reduced and so also will be N^* or $k[h-y(b,0)]/M$. However, the beam-stop configuration is not altered so that $[h-y(b,0)]$ is constant. Hence, M or the amplitude of the impact force will increase disproportionately.

Design considerations related to chatter are

illustrated next by employing the particular example associated with Figure 11. The stop is located below the beam's static equilibrium position and condition (A2.4) is satisfied. Now condition (A2.4) indicates a certain range of the beam's total kinetic energy, T, for which chatter can occur. Providing T is within this range, the beam will generally continue moving downwards immediately after an impact. Now a lower value of T indicates an overall lessening of inertia which will presumably reduce the downward tendency and decrease the amplitude of subsequent chatter. Therefore, one method of alleviating chatter would be to diminish the vibroimpacting beam's kinetic energy immediately before an impact. Table 2 suggests that this can be achieved, for example, by increasing the magnitude of the initial negative vertical distance, h, (i.e. reducing the original separation) between the stop and the beam's static equilibrium position. Further corroboration of this point can be obtained by comparing the $K^*=2.18\times10^4$ results shown in Figure 12 with those presented in Figure 13. Events after the corresponding first impacts happen at different times of course because of the different clearances of -0.125 and -0.3 inches, respectively, in Figure 12 and 13. However, it can be seen

clearly that the normalized tip displacement is generally much smaller in Figure 13. Consequently, as expected, the amplitude of chatter is much less for h=-0.3 inches than for h=-0.125 inches.

The vibroimpacting beam of reference [1] was used to assess the viability of the economical technique developed in Section 1.2.b. Results corresponding to two extreme values of K* and various values of h* are compared in Figure 14. Dashed lines correspond invariably to reference data whilst the continuous lines present analogous results predicted by the economical technique. Each reference case required approximately fifteen minutes of execution time on an Amdahl 470/V7 main frame computer. All the economically predicted results were obtained by extrapolation from the reference combination of $N_1^*=317$, $h_1^*=0.78$ and $K_1^*=2.18\times10^4$† . Equation (21) was employed to obtain, for $K_1^*=2.18\times10^4$, values of N* in Figure 14a corresponding to the different values of h*. Equation (22a) was then used to obtain N_2^* for $K_2^*=4.38\times10^4$ and h_1^*. Then equation (21) was again used to obtain the remaining points of Figure 14b. Operations associated with equation (21) and (22) were performed on a programmable calculator which produced tremendous computational

† Subscripts designate a particular combination of N*,K* and h*.

savings. Even so, Figure 14 indicates that the reference and predicted results agree well.

CONCLUSIONS

An approximate technique was developed to determine the flexural response of a vibroimpacting beam. The accuracy of the technique was assessed by using an example in which the beam's external excitation was a sinusoidal point load. The results showed that the technique significantly reduces computational effort yet largely preserves accuracy. This accuracy can be improved by combining the approximate with a purely numerical approach to predict the details of late contact forces. Problems associated with a user-friendly presentation of the dynamic interactions between a beam and stop were also outlined.

Although the approximate technique provided a quick computationally efficient overview, its use did not produce fine details like chatter. Therefore, an energy criterion was suggested by which the possibility of *chatter* may be predicted from a priori information. Several illustrations of rapid collisions tended to substantiate the criterion.

An economical approach was then developed to predict practically important maximum impact forces yet decrease the computational effort in design situations where the material or clearance parameters of an invariant

configuration may be changed. The main novelty in the approach lay in the effective use of a set of non-dimensional vibroimpact parameters from the equations of motion. This allowed an extrapolation from the results of any one given combination of vibroimpact parameters. The viabilty of the approach was assessed by using a vibroimpacting beam example with no external load. The approach produced tremendous computational savings. Even so, reference and predicted results agreed well.

A combination of all approaches can be used economically to optimally design vibroimpact stops. The energy criterion can be employed to check design alternatives with respect to the occurrence of chatter and its amplitude. The criterion only requires knowledge of a beam-like structure's total kinetic and strain energies just before an impact. These values are a function of the structure's displacement and velocity and can be predicted quite accurately by using the approximate technique. The magnitude of an impact force corresponding to different combinations of vibroimpact variables can then be extrapolated from any one computed case by using the economical approach. Finally, when a stage close to the

final design has been reached, ultra accurate histories can always be computed numerically.

CHAPTER 2
INTRODUCTION

High impact stresses associated with snubbers have led to alternatives being considered for controlling the seismic response of piping systems . These alternatives are essentially ductile materials which are designed to yield under severe dynamic conditions. Hence, control would be achieved by a virtually inelastic rather than the elastic action of a snubber. Furthermore, the continuous contact of the ductile device will presumably reduce the stress penalty inherent to the snubber's intermittent action. The feasibilty of using this approach has been partially explored experimentally [17-19]. Piping was modelled either as a plane or spatial frame in reference [17] and reference [18-19], respectively. It was reported in reference [17] that substantial yielding of ductile restrainers lowered a frame's fundamental natural frequency due to the hysteretic action of the yielding devices. (It was also claimed that this action substantially increased the damping.) However, it was found in reference [19] that a restrainer's effective stiffness , which depends upon the amount of deformation, increased a piping system's natural frequencies. A similar conclusion can be drawn from the Fast Fourier Transform

(FFT) results reported in reference[17]. It was also observed that whilst the fundamental mode dominated the response when the spatial piping was restrained inelastically this was not the case with rigid restraints [19]. Schneider et al [19] compared the experimental behaviour of a spatial piping system restrained by either snubbers or yielding materials. As expected, snubbers were found to limit the pipe's motion but, unlike inelastic restrainers, they induced high frequency energy in the piping and gave a large stress penalty. On the other hand, properly chosen inelastic restrainers reduced the stresses but were ineffective in attenuating the motion of the pipe. In all the reported experimental work [17-19], the selected piping systems were excited by means of the shaking table at the Earthquake Engineering Research Center (EERC), University of California at Berkeley. The time histories fed to the shaker were based on the TAFT earthquake which has a broad frequency spectrum. However, the measured response spectra of the shaking table were different from the actual earthquake . Large displacements at frequencies less than 0.2 Hz and small displacements at frequencies greater than about 10 Hz were both effectively filtered out due to the table's properties.

The present work reports the results of an analytical study which was conducted to complement previous experimental work and assess the effectiveness of inelastic restrainers. The mathematical model was developed by using a finite element approach. It is general in terms of piping geometry, location and number of restrainers. In addition, the model permitted a comparison between the performance of elastic and inelastic restrainers. "Dynamic" condensation [20] was introduced to reduce the computational effort required in the numerical evaluation of the equations of motion. An example is presented wherein a two-dimensional U-frame was subjected to a filtered and unfiltered TAFT S69E earthquake loading. Results tend to show that yielding materials are ineffective as energy absorbers.

THEORY

The dynamic response of an s degree-of-freedom structural system can be represented by [14]

$$[M]\{u''(t)\} + [C]\{u'(t)\} + [K]\{u(t)\} = \{F(t)\} \quad (23)$$

where [M],[C] and [K] are the time invariant global mass, damping and stiffness matrices, respectively. Their sxs elements are usually determined by using a standard finite element approach [14]. The sx1 {F(t)} and {u(t)} matrices, on the other hand, correspond to the time dependent load and displacement vectors, respectively. A dot superscript denotes differentiation with respect to time, t.

Because of the geometrical non-linearities inherent to restrained piping systems, elements of stiffness matrix [K] undergo changes during the dynamic response which alter the vibration characteristics. Therefore, normal coordinate uncoupling of equation (23) is not straightforward [14]. Consequently, numerical step-by-step integration of the coupled equations is often used. Then calculations are performed by assuming the system to be linear in a suitably short period ,Δt. However, the stiffness may change at the end of the period so that a

non-linearity is treated essentially as a series of linear characteristics. Time increments, Δt, are usually identical. Therefore, the equilibrium of forces requires

$$[M]\{u''(t+\Delta t)\} + [C]\{u'(t+\Delta t) + [K]\{u(t+\Delta t)\} = \{F(t+\Delta t)\} \cdot \quad (24)$$

Subtracting equation (23) from equation (24) yields the incremental form of the equations of motion as

$$[M]\{\Delta u''\} + [C]\{\Delta u'\} + [K]\{\Delta u\} = \{\Delta F\} \cdot \quad (25)$$

The basic operation of the step-by-step solution is the conversion of differential equations (25) to a set of simultaneous algebraic equations. This procedure can be accomplished by introducing a simple relationship between the displacement, velocity and acceleration which is assumed valid over Δt. Then the change in velocity and acceleration can be expressed in terms of the incremental displacement. Consequently, only one unknown vector remains in the incremental equilibrium equation. It can be evaluated by a standard simultaneous equation solution procedure like the Cholesky Method [24]. Recursive relations for displacements and velocities, which are

determined more conveniently in Appendix A3, convert equation (25) to the following simultaneous equations

$$[\tilde{K}]\ \{\Delta u\} = \{\Delta\tilde{F}\}. \qquad (26)$$

Here $\{\Delta\tilde{F}\}$, the effective incremental load vector, is time dependent and, therefore, has to be calculated at the beginning of each time step. The$[\tilde{K}]$ or effective stiffness matrix is a function of the time increment Δt. If the latter remains unchanged throughout, $[\tilde{K}]$ will need calculating only once for a completely linear system. On the other hand, $[\tilde{K}]$ will be usually different from one step to another for a geometrically non-linear system and, therefore, will need to be updated correspondingly.

The practical problem of using physical restrainers to control the behaviour of piping systems can be solved in principle by using the previously described approach. However, the cost of updating the full stiffness matrix at the end of each time step can be prohibitive. Now the specific piping system to be considered here exhibits non-linearities only where the restrainers are positioned. Therefore, the non-linearities are localised which makes feasible the use of "substructuring" to significantly

reduce computational effort [21]. For convenience, the degrees of freedom pertaining to the time dependent elements of $[\tilde{K}]$ will be called "non-linear" whilst the remainder will be termed "linear". Substructuring essentially decomposes the linear from the non-linear components in equation (26) so that

$$[\tilde{K}'] \begin{Bmatrix} \{\Delta u_{NL}\} \\ \{\Delta u_{L}\} \end{Bmatrix} = \begin{Bmatrix} \{\Delta \tilde{F}_{NL}\} \\ \{\Delta \tilde{F}_{L}\} \end{Bmatrix} \qquad (27)$$

where suffix "NL" and "L" correspond to the linear and non-linear degrees-of-freedom, respectively. The $\{\Delta u_L\}$ are condensed at the beginning of the step-by-step solution by performing a symmetric backward Gaussian elimination [22] on equation (27). Consequently, only r equations need be solved in each time step where r is the number of non-linear degrees-of- freedom. The elimination can be programmed efficiently for p=s,s-1,s-2,.....(r+1) by using the following operations on equation (25)

$$\left.\begin{aligned}(\tilde{K}_{ij})_{NEW} &= \tilde{k}_{ij} - \tilde{k}_{ip}\,\frac{\tilde{k}_{pj}}{\tilde{k}_{pp}} \\ (\Delta\tilde{F}_j)_{NEW} &= \Delta\tilde{F}_j - \tilde{K}_{jp}\,\frac{\Delta F_p}{\tilde{K}_{pp}}\end{aligned}\right\} \qquad (28)$$

$$j=1,2,\ldots\ldots,p-1$$
$$i=j,j+1,\ldots,p-1 \ .$$

Operations associated with equation (28) generate the lower triangle of the $[\tilde{K}]$ matrix. The upper triangle is obtained implicitly by enforcing symmetry. This procedure resembles "static" condensation [20] thus far except that the recovery of the condensed degrees-of-freedom has to be performed at each time step rather than at the end of the complete solution. The recovery is accomplished by the forward substitution

$$(\Delta u_i) = \frac{(\Delta\tilde{F})_{NEW} - \sum_{j=1}^{i-1} (\tilde{K}_{ij})_{NEW}\ \Delta u_j}{(\tilde{K}_{ii})_{NEW}} \qquad (29)$$

$$i = r+1,r+2,\ldots\ldots\ldots,s.$$

The outlined procedure has been implemented on an IBM PC computer equipped with 128 k-bytes of memory and a UCSD p (operating) system [23]. The developed program could predict quite accurately the experimental results

reported in references [3] and [4].

RESULTS AND DISCUSSION

The results presented here are based upon the algorithm described in the previous section. The vibrating system selected was basically a plane frame with a U-configuration similar to that used in reference [17]. The system was supported rigidly at the two ends of the U, as shown in Figure 15b. All the material properties of the frame and other related constants are given in Figure 15. The finite element model of the frame consisted of three elements each having two displacements and one angular rotation at a node [24]. The Newmark-β method [25] was used to convert the incremental form of the equations of motion to a system of simultaneous equations. The time increment, Δt, was chosen equal to 1/10th the fundamental natural period of the frame. Both the actual and filtered TAFT S69E seismic histories were used as exciting loads. The filtered history was obtained by digitizing the response of the shaking table reported in reference [17]. Acceleration spectra† of both histories are presented, for convenience, in Figure 16 where it can be seen that the actual earthquake has a broader frequency spectrum than the filtered one. The inelastic restrainer was simulated by a yielding material having the general load-displacement characteristics shown in Figure 17a.

---

† The acceleration spectra, reprted in this section, were calculated by using the FFT algorithm of reference [26].

The material's character may be represented by a bilinear hysteretic loop which can be described by the stiffnesses k_1 and k_2 and the yield displacement, x_y. The area enclosed by the loop represents the hysteretic energy dissipated per cycle. It equals $4(k_1-k_2)(x_y x_{max}-x_y^2)$ where x_{max} is the maximum displacement of the restrainer during the cycle. One restrainer alone was used at the location (the corner and in the same plane as the U-loop) where the maximum displacement was anticipated. Only the peak dynamic response is of interest in the present work because the primary objective of restrainers is to limit transient excursions of the piping. An isometric illustration of the piping system showing the restrainer location is given in Figure 15c .

The system shown in Figure 15 was excited horizontally in the plane of the frame by applying the filtered TAFT S69E earthquake to the rigid supports. It was generally observed that the fundamental mode of the system dominated the dynamic response. The acceleration spectra of the unrestrained and restrained system are presented in Figure 18. The restrainer consists of a yielding material with stiffnesses k_1 and k_2 of 3000 and 1500 lb_f/in, respectively, and a yielding displacement,

x_y, equal to 0.11 inches. The results show that the restrained system's response was lower. Several additional results were then generated for the restrained case with k_1 and k_2 kept constant whilst the x_y was varied from 1.0 to 10.0 inches. The objective was to determine the effect of the dissipated hysteretic energy. Acceleration spectra corresponding to x_y equal to 1, 5 and 10 inches are displayed in Figure 19a, b and c, respectively. It can be seen from the main peaks that increasing x_y from 1 to 5 inches, or equivalently increasing the amount of energy dissipation, reduced the system's response. However, a further increase to 10 inches hardly changed the peaks. It can also be observed from the frequency shift of the global peak that the fundamental natural frequency of the system generally increased slightly with a rise in x_y. This implies that the behaviour of the whole system is stiffness controlled. Such an observation raises the question of what is really causing the reduction? Could the system's response be reduced by strictly adding stiffness through an elastic restrainer ? Alternatively, is some restrainer deformation and, hence, energy dissipation essential ? These questions are answered best by introducing a hypothetical restraining material which yields but does not dissipate

energy (i.e. the area enclosed by the hysteresis loop is set to zero.) Such a material has the general load-displacement characteristics shown in Figure 17b . Acceleration spectra of the system restrained by a hypothetical material having the same stiffnesses as the true yielding material but with x_y equal to 5 and 10 inches are shown in Figure 20a and b, respectively. The close similarity between these results and those in Figure 19 corresponding to the actual yielding material clearly indicates that the dissipated energy has virtually no effect. Therefore, the reduction in the dynamic response is due solely to the frequency shift resulting from the additional stiffness of the restrainer. This finding is explained by comparing the unrestrained and restrained system's acceleration spectra displayed in Figure 18a and 18b for the filtered earthquake of Figure 16a. A careful examination of Figure 16a and 18a will reveal that the fundamental natural frequency of the unrestrained system corresponds to a relatively high magnitude of the earthquake's spectral acceleration. The additional stiffness of the restrainer slightly increases the system's natural frequency and makes it coincide with a lower spectral peak. This results, in turn, to the

reduction in the dynamic response. However, by the same reasoning, a response amplification could have ensued if the frequency is shifted to coincide with a higher spectral peak of the filtered earthquake. Recalling that the filtered spectrum is quite narrow, it may be suggested that the same restrainer may not be so effective for the actual (broad) spectrum inherent to the TAFT earthquake.

The system of Figure 15 was excited by using data corresponding to the actual rather than the filtered TAFT earthquake. Again, it was found that a close similarity exists between the spectra corresponding to the true and hypothetical yielding materials . On the other hand, a comparison between the acceleration spectra in Figure 21 indicates that the system's peak response has undesirably increased after restraint. This simply means that a frequency shift is beneficial in some cases but not in others. The outcome depends totally upon the relation between the fundamental natural frequency of the system and the frequencies contained in the seismic excitation. However, it is difficult to accurately predict the frequency content of earthquakes due to their unreliable nature. Therefore, there will be no guarantee that an inelastic device will always be effective.

It was shown previously that the energy dissipated by the yielding material is too small to be considered valuable in reducing the system's peak response. This observation can also be substantiated by considering the more commonly used equivalent viscous damping ratio, ζ_{eq}. Hadjian [26] has shown the adequacy of the model proposed by Iwan [27] for predicting equivalent damping values of non-linear systems subjected to earthquake excitations. The damping equivalent to the hysteretic action of a yielding material is given by the empirical relationship [32]

$$\zeta_{eq} = 0.0587 \left[\frac{x_{max}}{x_y} - 1 \right]^{0.371} \qquad (30)$$

where x_{max} is the maximum amplitude of the response and x_y is the associated yielding displacement. The ζ_{eq} was found to equal only 5% for the present piping example when excited by the actual TAFT earthquake and restrained by a material with a fairly representative yielding of 5.0 inches. Such a small percentage cannot be expected to contribute significantly to a reduction in the piping system's peak response. It can certainly be argued that insufficient deformation was allowed for this particular

example so that no significant energy was dissipated. However, such an argument contradicts the main objective of restraints which is essentially to limit excessive transient excursions of the vibrating system.

CONCLUSIONS

A comprehensive study was conducted to complement previous experimental work and assess the effectiveness of inelastic restrainers. The theoretical model was developed by using a finite element approach and it is general in terms of piping geometry, location and number of restrainers. Dynamic condensation was introduced to reduce the computational effort required in the numerical evaluation of the equations of motion. An example was presented wherein a two-dimensional U-frame was subjected to a filtered and unfiltered TAFT S69E earthquake loading. The results tend to discourage the use of ductility for damping seismically induced excursions of piping systems. However, a yielding material has the potential of being efficient if utilised as a force-limiting device rather than a damper. This latter characteristic could be employed advantageously only if the inelastic device was positioned to isolate the mechanical system from the earthquake. Then any exciting energy would be capped before reaching the system. Snubbers could be employed if undesirably excessive deflections still potentially exist. The combined use of elastic and inelastic devices may be advantageous because the stress penalty associated with a snubber would be alleviated as a result of reducing the

input energy.

CHAPTER 3
RECOMMENDATIONS FOR FURTHER STUDIES

Three computationally efficient approaches were developed to approximately determine the flexural response and important design parameters of vibroimpact systems. A combination of the three approaches can be used economically to to reach optimum designs. However, the applicability and accuracy of these approaches was only explored for vibroimpacting beams. Therefore, the feasibilty of extending these approaches to more complicated systems should be investigated.

A study was conducted to assess the use of inelastic restrainers for damping seismically induced excursions of piping systems. The results introduced doubts about the effectiveness of these restrainers when used as energy absorbers. This finding needs to be more thouroughly investigated by doing more exhaustive comparisons using , for example, random excitation. In addition, the inelastic restrainers have the potential to function as an input force limiting device. This potential is to be explored.

REFERENCES

1. R.J.Rogers and R.J.Pick 1976 Nuclear Engineering and Design 36, 81-90. On The Dynamic Spacial Response Of A Heat Exchanger Tube With Intermittent Baffle Contacts.

2. F.P. Beer and E.R.Johnston,Jr. 1981 Mechanics of Materials. McGraw-Hill Inc.

3. Y.A.Mariami,S.F.Masri and J.C.Anderson 1980 NUREG/CR-1318, U.S. Nuclear Regulatory Commission, Washington, D.C. Analytical and Experimental Studies of a Beam with a Geometric Non-linearity.

4. C.C.Lo 1980 Journal of Sound and Vibration 69, 245-255. A Cantilever Beam Chattering Against a Stop.

5. S.Timoshenko, D.H.Young and W.Weaver,JR, 1974 Vibrations Problems In Engineering. John Wiley and Sons, Inc.

6. G.B.Warburton 1976 The Dynamical Behaviour Of Structures, Pergamon Press.

7. Y.S.Shin,D.E.Sass and J.A.Jendrzejczyk 1978 ASME-CSME Conference on Pressure vessels and Piping, Montreal, Quebec. Vibroimpact Responses Of A Tube-Baffle Interaction.

8. C.R.Eddie 1970 18th Annual, National Relay Conference, Oklahoma State University, Stillwater, Oklahoma. Finite Element Analysis Of Relay Chatter.

9. C.L.Elliott and R.J.Pick 1974 3rd International - 22nd annual National Relay Conference at Oklahoma State University, Stillwater, Oklahoma. Parametric Analysis Of Contact Chatter In Relays.

10. R.R. Craig,Jr. 1981 Structural Dynamics. John Wiley & Sons Inc.

11. E.H.Lee 1940 Journal of Applied Mechanics 7, 129-138. The Impact Of A Mass Striking A Beam.

12. C.Sundararajin,A.K.Vaish and G.C.Slagis 1981 Winter Annual Meeting of The Pressure Vessel And Piping Division, ASME, Washington D.C. Seismic Analysis Of Piping Systems Subjected To Multiple Support Excitations.

13. H.G.Davies 1978 Journal of Sound and Vibration 68-4, 479-487. Random Vibrations Of Beam Impacting Stops.

14. R.W.Clough and J.Penzien 1975 Dynamics of Structures McGraw-Hill Inc.

15. R.E.D.Bishop and D.C.Johnson 1960 The Mechanics Of Vibration. The Syndics of the Cambridge University Press.

16. M.A.Pickett and J.R.Gartner 1981 Winter Annual Meeting of The Pressure Vessel And Piping Division, ASME, Washington D.C. Development Of Non-Linear Frequency And Load Dependent Models For Snubbers.

17. S.F.Steimer, and W.G.Godden 1980 UCB/EERC-80/33. Shaking Table Tests Of Piping Systems With Energy Absorbing Restrainers.

18. S.F.Steimer W.G.Godden and J.M.Kelly 1981 UCB/EERC-81/09. Experimental Behaviour Of A Spacial Piping System With Steel Energy Absorbers Subjected To A Simulated Differential Seismic Input.

19. S.Schneider, H.M.Lee and W.G.Godden 1981 UCB/EERC. Piping Seismic Test With Energy Absorbing Devices.

20. C.S.Desai and J.F.Abel 1972 Introduction to The Finite Element Method. Van Norstrand Reinhold, New York.

21. K.J.Bathe and S.Gracewski 1981 Computer and Structures 13, 669-707. On Non-linear Dynamic Analysis Using Substructuring and Mode Superposition.

22. M.L.James, G.M.Smith and J.C.Wolford 1977 Applied Numerical Methods for Digital Computation with FORTRAN and CSMP. T.Y. Crowell Company Inc.

23. C.W.Grant and J.Butah 1982 Introduction to the UCSD p-System. Sybex Inc.

24. S.S.Rao 1982 The Finite Element Method in Engineering. Pergamon Press.

25. N.M.Newmark 1959 Journal of Engineering Mechanics Division, ASME, EM3, 67-94.A Method Of Computation For Structural Dynamics.

26. J.F. Hall 1982 Earthquake Engineering and Structural Dynamics 10 ,797-811. An FFT Algorithm For Structural Dynamics.

27. A.H.Hadjian 1982 Earthquake Engineering and Structural Dynamics 10, 759-767. A Re-evaluation of Equivalent Linear Models for Simple Yielding Systems.

28. W.D.Iwan 1980 Earthquake Engineering and Structure Dynamics **8**, 375-388. Estimating Inelastic Response Spectra.

29. K.J.Bathe and E.L.Wilson 1973 Earthquake Engineering and Structural Dynamics **1**, 283-291. Stability and Accuracy Analysis Of Direct Integration Methods.

30. N.M.Newmark and E.Rosenblueth 1971 Fundamental of Earthquake Engineering. Prentice Hall Inc., Englewood Cliffs, N. J.

31. A.C.Ugural and S.K.Fenster 1981 Advanced Strength and Applied Elasticity. Elsevier North Holland Inc.

32. R.F.Steidel,Jr. 1979 An Introduction to Mechanical Vibrations. John Wiley and Sons Inc.

33. P.C.Jennings 1968 Journal of Engineering Mechanics Division **EM1**, 103-116. Equivalent Viscous Damping for Yielding Structures.

34. R. Burton 1968 Vibration and Impact. Dover PublicationsInc.

35. R.L.Wiegel 1970 Earthquake Engineering. Prentice Hall Inc. Englewood, Cliffs, N.J.

APPENDIX A1

If the amplitude, Q, of the external load is sufficiently large that impacts occur in the example of Figure 3, then the equation of motion during contact is

$$m\,Z''(t) + (K+k)\,Z(t) = Q \sin \Omega t + kZ_1 \qquad (A1.1)$$

The Z(t) represents the displacement of mass m and a dot superscript indicates differentiation with respect to time, t. The solution of equation (A1.1) is given in reference [5] as

$$Z(t) = \begin{cases} \left[Z_1 - \dfrac{Q \sin \Omega t_o}{(k+K)\ (1-\beta^2)} \right] \cos \omega'_n (t-t_o) \\ + \left[\dfrac{\dot{Z}_1}{\omega'_n} - \dfrac{Q\beta \cos \Omega t_o}{(K+k)\ (1-\beta^2)} \right] \sin \omega'_n (t-t_o) \\ + \dfrac{Q \sin \Omega t}{(k+K)\ (1-\beta^2)} + \dfrac{kZ_1}{(k+K)} \left[1 - \cos \omega'_n (t-t_o) \right] \end{cases} \qquad (A1.2)$$

where Z_1 and $\dot{Z}_1$ are the displacement and velocity, respectively of the oscillator at the first instant, t_o, it contacts the stop. The natural frequency ω_n' equals $[(K+k)/m]^{1/2}$ and $\beta = \Omega/\omega'_n$. Now the primary use of the stops occurs in practice when the oscillator alone is close to resonance so that Ω equals $(K/m)^{1/2}$. Then

$$\beta = \frac{\Omega}{\omega'_n} = \frac{1}{\left[1 + \frac{k}{K} \right]^{1/2}} \quad . \qquad \text{(A1.3)}$$

For stiff stops, $k/K \gg 1$ and, hence, it can be seen from equation (A1.3) That β is much less than unity. Consequently, equation (A1.2) then reduces to

$$Z(t) = \left\{ \begin{array}{l} Z_1 \cos \omega'_n(t-t_o) \\ + \frac{kZ_1}{(k+K)} \left[1 - \cos \omega'_n(t-t_o) \right] \\ + \left[\frac{\dot{Z}_1}{\omega'_n} - \frac{Q}{k} \left[\frac{k}{k+K} \right]^{1/2} \right] \sin \omega'_n(t-t_o) \end{array} \right. \quad . \qquad \text{(A1.4)}$$

The contact force is simply

$$N(t) = (K+k)\, Z(t) \qquad \text{(A1.4)}$$

which, by using approximation (A1.3), becomes

$$N(t) = \left[m\dot{Z}_1 - \frac{Q}{k} (km)^{1/2} \right] \omega'_n \sin \omega'_n(t-t_o) \quad . \qquad \text{(A1.5)}$$

The form of equation (A1.5) suggests that the contact force, N(t), is half sinusoidal in form for a single

oscillator colliding against a stiff stop. Consequently, equation (A1.5) may be rewritten in the more convenient abbreviated form

$$N(t) = A \sin ft \qquad \text{(A1.6a)}$$

where

$$A = \omega'_n \left[m\dot{Z}_1 - \frac{Q}{k} (km)^{1/2} \right], \qquad \text{(A1.6b)}$$

and

$$ft = \omega'_n (t - t_o) \quad .$$

Appendix A2

Energy criterion for predicting the possibility of chatter

The physics of the chatter phenomenon can be understood best by studying the vibrating structure's total energies. Consider, for example, the transverse vibration of a cantilevered beam deflected initially above an elastic stop. The beam first travels downwards or towards the stop after release. A point spring force is generated at the impact which momentarily forces the beam's point of contact upward. Subsequent travel will depend upon the beam's overall kinetic and strain energies and the stop's location. If the stop is located above the beam's static equilibrium position, both the kinetic and strain energies will induce the beam's non-contact points to move downwards. This means that when the stop and the beam's point of contact are separated, the latter will move again (along with the non-contact points) towards the stop. Hence, as long as the beam moves downwards after contact, the beam's likely point of contact will go through a fairly rapid succession of contacts and non-contacts or "chatter" with the stop. On the other hand, if the stop is located below the beam's static equilibrium position, then the beam's kinetic and strain energies will have counterbalancing influences. While the kinetic

energy induces the beam to travel downwards , the strain energy tends to return it back to the static equilibrium position. Therefore, if the kinetic energy is greater than the strain energy just before a contact, the beam moves downwards so that chatter will take place. Hence the condition for chatter can be expressed mathematically as

$$T > U \qquad (A2.1)$$

where T and U are the beam's total kinetic and potential energies, respectively, immediately before the contact. The total energy (T+U) remains constant for a conservative system so that

$$T + U = \text{constant} = E_T \ . \qquad (A2.2)$$

Accordingly U can be expressed in terms of T and E as

$$U = E_T - T$$

and, hence, inequality (A2.1) can be expressed alternatively as

$$T > \frac{1}{2} E_T \quad . \qquad \text{(A2.3)}$$

However, T cannot exceed the total energy E_T. Therefore, inequality (A2.3) can also be written in the form

$$\frac{1}{2} E_T < T \leq E_T \quad . \qquad \text{(A2.4)}$$

In summary, the possibility of chatter depends upon the stop's location relative to the beam's static equilibrium position and the beam's total kinetic and strain energies just before a contact. Chatter occurs if the stop is located above the beam's static equilibrium position. If the stop is located below this position, chatter only occurs if condition (A2.4) is satisfied immediately prior to the contact.

APPENDIX A3

The incremental form of equation (23) is

$$[M]\{\Delta u^{\cdot\cdot}\} + [C]\{\Delta u^{\cdot}\} + [K]\{\Delta u\} = \{\Delta F\} \cdot \qquad (A3.1)$$

By using recursive relations based on a Taylor series expansion, the incremental variables of equation (A3.1) can be expressed in series form as

$$\begin{aligned}\{\Delta u\} &= \{u(t+\Delta t)\} - \{u(t)\} \\ &= \{u^{\cdot}(t)\}\Delta t + [(1/2-\beta)\{u^{\cdot\cdot}(t)\} + \beta\{u^{\cdot\cdot}(t+\Delta t)\}]\Delta t^{2} \\ &= \{u^{\cdot}(t)\}\Delta t + \{u^{\cdot\cdot}(t)\}\Delta t^{2}/2 + \{\Delta u^{\cdot\cdot}\}\Delta t^{2}\beta\end{aligned} \qquad (A3.2)$$

and

$$\begin{aligned}\{\Delta u^{\cdot}\} &= \{u^{\cdot}(t+\Delta t)\} - \{u^{\cdot}(t)\} \\ &= [(1-\gamma)\{u^{\cdot\cdot}(t)\} + \gamma\{u^{\cdot\cdot}(t+\Delta t)\}]\Delta t \\ &= \{u^{\cdot\cdot}(t)\}\Delta t + \{\Delta u^{\cdot\cdot}\}\Delta t\gamma \cdot\end{aligned} \qquad (A3.3)$$

The choice of parameters β and γ, which appear in expression (A3.1) and (A3.3), stems from the acceleration's assumed variation with time during the interval Δt. A linear variation, which corresponds to the

Wilson-θ method [28], arises from $\beta=1/6$ and $\gamma=1/2$. On the other hand, the Newmark-β method [25] is synonymous with a constant average acceleration which emanates from $\beta=1/4$ and $\gamma=1/2$.

The incremental acceleration $\{\Delta u''\}$ can be obtained from expression (A3.2) as

$$\{\Delta u''\} = \frac{1}{\beta\Delta t^2}\{\Delta u\} - \frac{1}{\beta\Delta t}\{u'(t)\} - \frac{1}{2\beta}\{u''(t)\} \quad . \quad \text{(A3.4)}$$

Substituting expression (A3.4) into (A3.3) yields

$$\{\Delta u'\} = \begin{cases} \{u''(t)\}\Delta t \\ + \gamma\Delta t\left[\frac{1}{\beta\Delta t^2}\{\Delta u\} - \frac{1}{\beta\Delta t}\{u'(t)\} - \frac{1}{2\beta}\{u''(t)\}\right] \end{cases} . \quad \text{(A3.5)}$$

By assuming that the damping matrix is proportional to the mass matrix, with a proportinal constant c, expression (A3.5) and (A3.4) may be substituted into equation (A3.1) to give

$$[\tilde{K}]\{\Delta u\} = \{\Delta\tilde{F}\} \quad \text{(A3.6)}$$

where $[\tilde{K}]$, the effective stiffness matrix, is

$$[\tilde{K}] = [K] + \frac{1}{\beta\Delta t}\left[\frac{1}{\Delta t} + c\gamma\right][M] \qquad (A3.7)$$

and $\{\tilde{F}\}$, the effective incremental load vector, has the form

$$\{\Delta\tilde{F}\} = \{\Delta F\} + [M]\left[\frac{1}{\beta}\left[\frac{1}{\Delta t} + c\gamma\right]\{u'(t)\} + \frac{1}{2\beta} + c\Delta t\left[\frac{\gamma}{2\beta} - 1\right]\{u''(t)\}\right]. \qquad (A3.8)$$

An integration cycle starts with known initial values for $\{u(t)\}$, $\{u'(t)\}$ and $\{u''(t)\}$. Values of $\{\Delta\tilde{F}\}$ and $[\tilde{K}]$ are calculated from equation (A3.6). The solution of equation (A3.6) will provide the $\{\Delta u\}$ which can be substituted into expression (A3.4) and (A3.5) to produce $\{\Delta u''\}$ and $\{\Delta u'\}$, respectively.

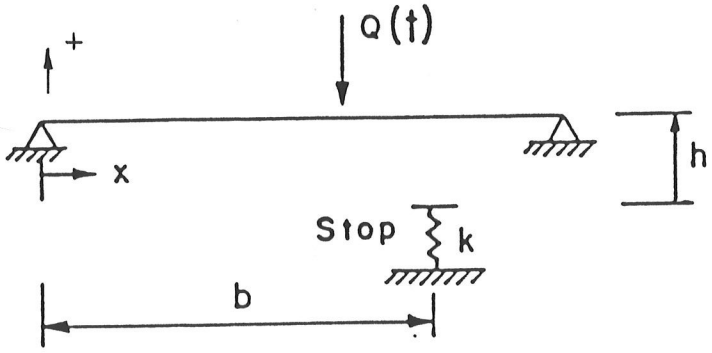

Figure 1. An overall illustration of a beam impacting against a resilient stop.

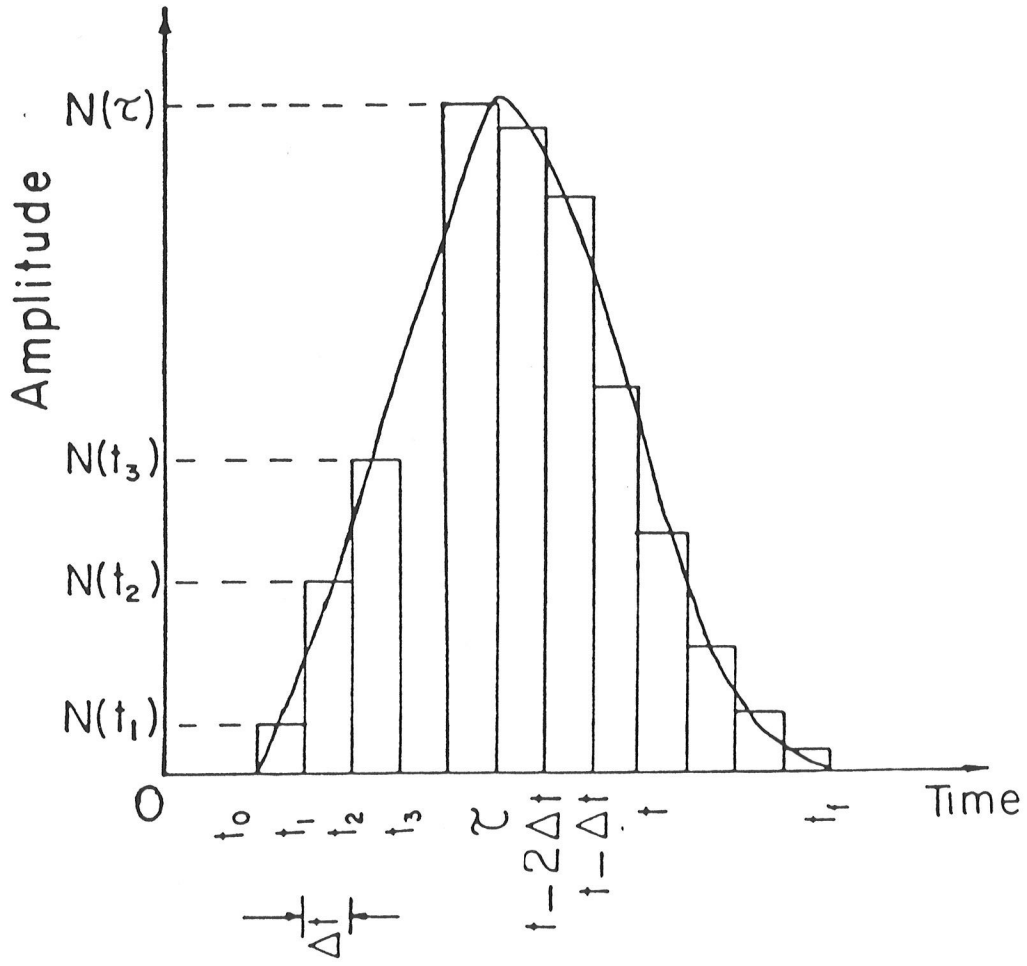

Figure 2. Idealization of a contact force by a sequence of impulses.

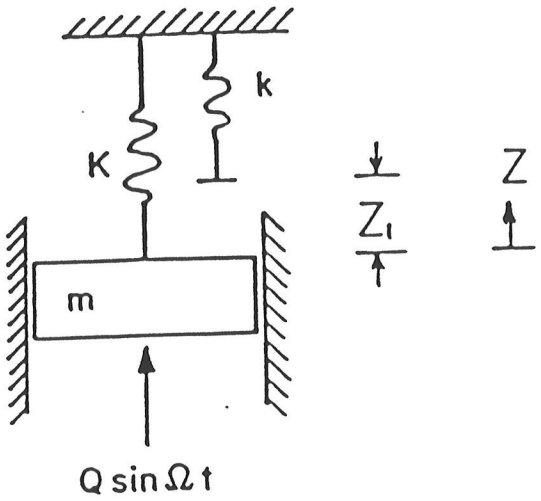

Figure 3. Showing an undamped oscillator colliding with a resilient stop.

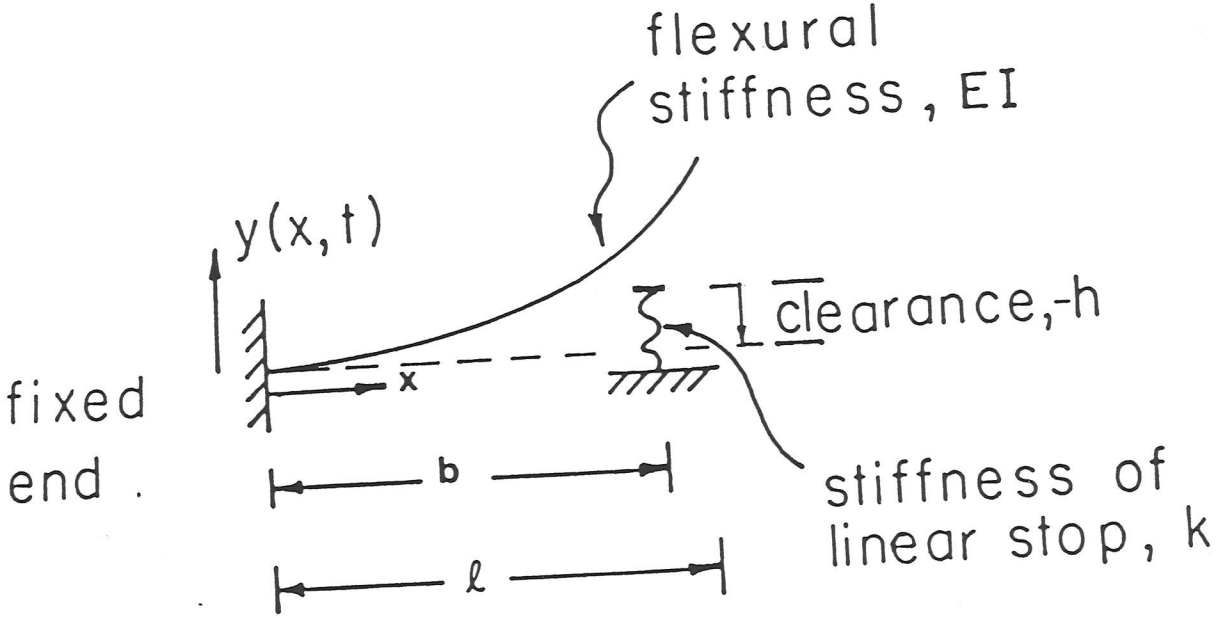

Figure 4. General material and geometrical properties used to describe a cantilevered beam colliding with a resilient stop.

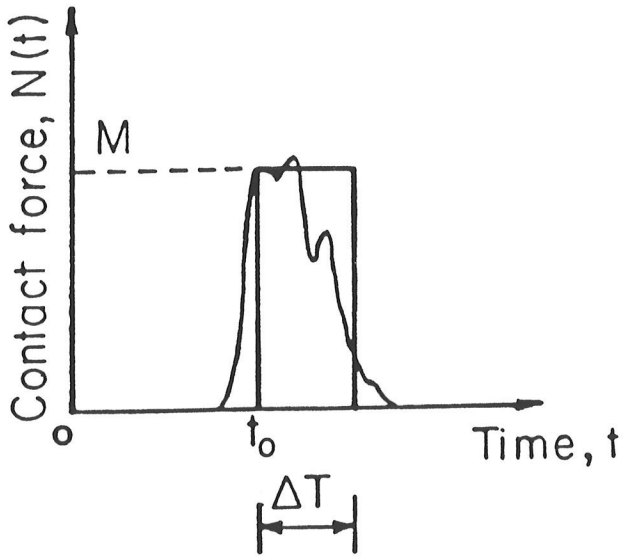

Figure 5. Pragmatic idealization of a contact force as a single rectangular pulse.

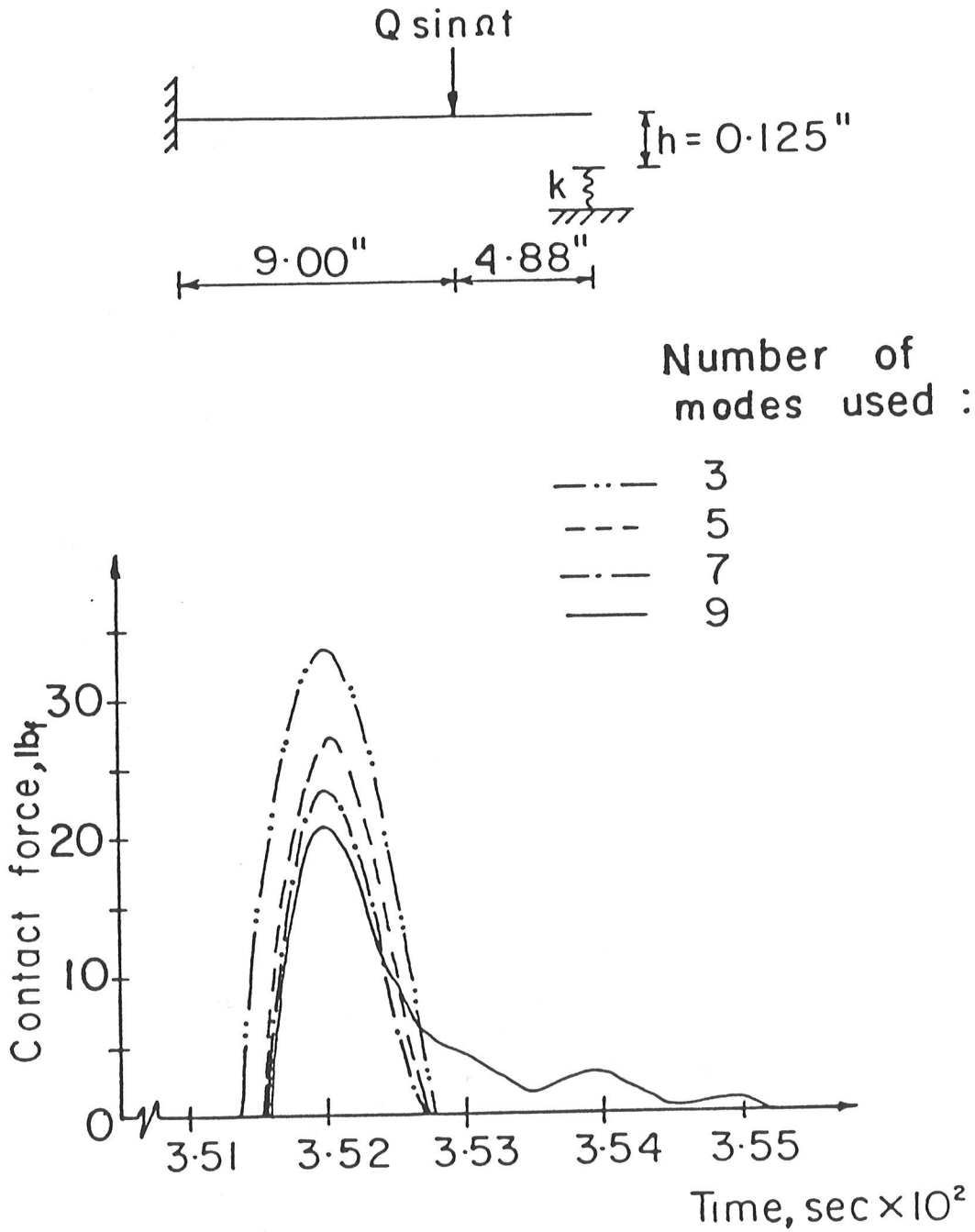

Figure 6. The effects of using a different number of modes to describe the first contact force of the externally loaded vibroimpact system of reference [2]. Additional system properties are given in Table 1.

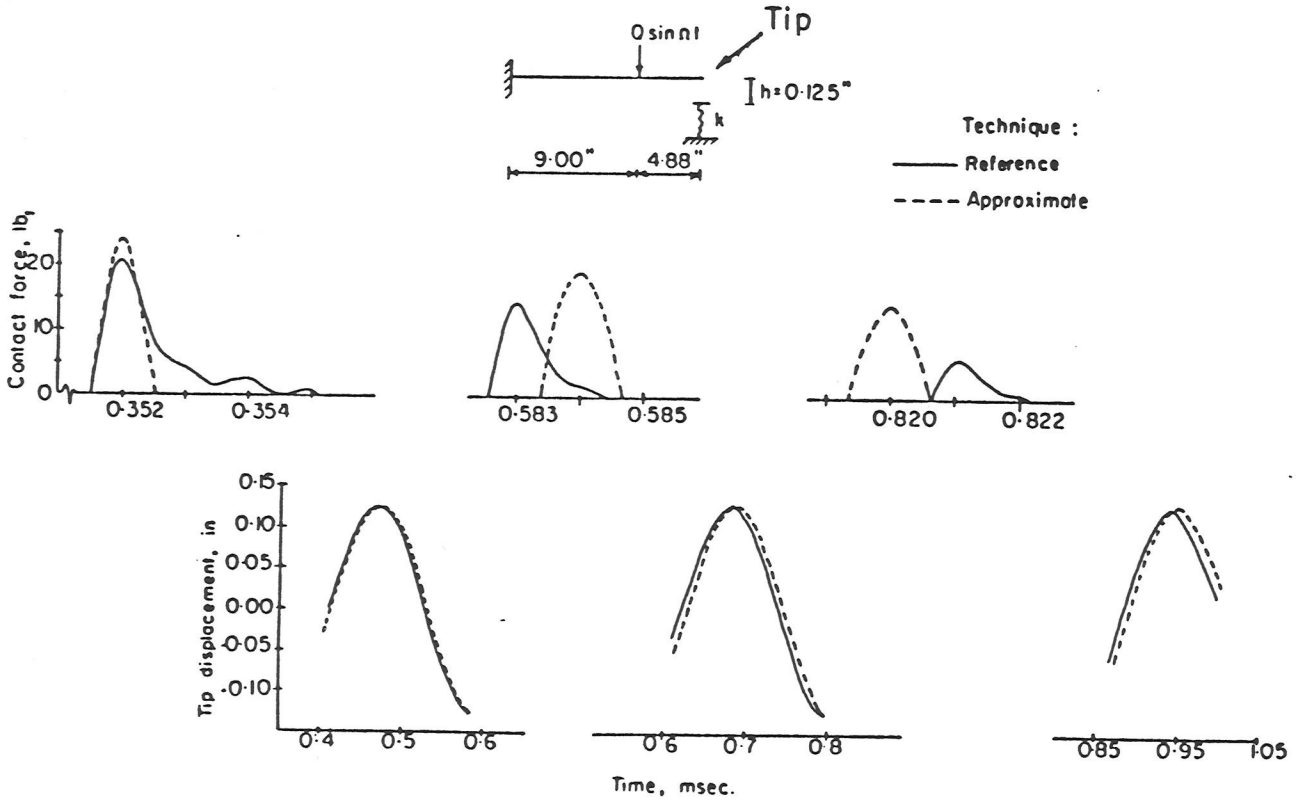

Figure 7. A comparison of the first three reference and approximate contact forces and displacement outcomes for the vibroimpact system of Figure 6.

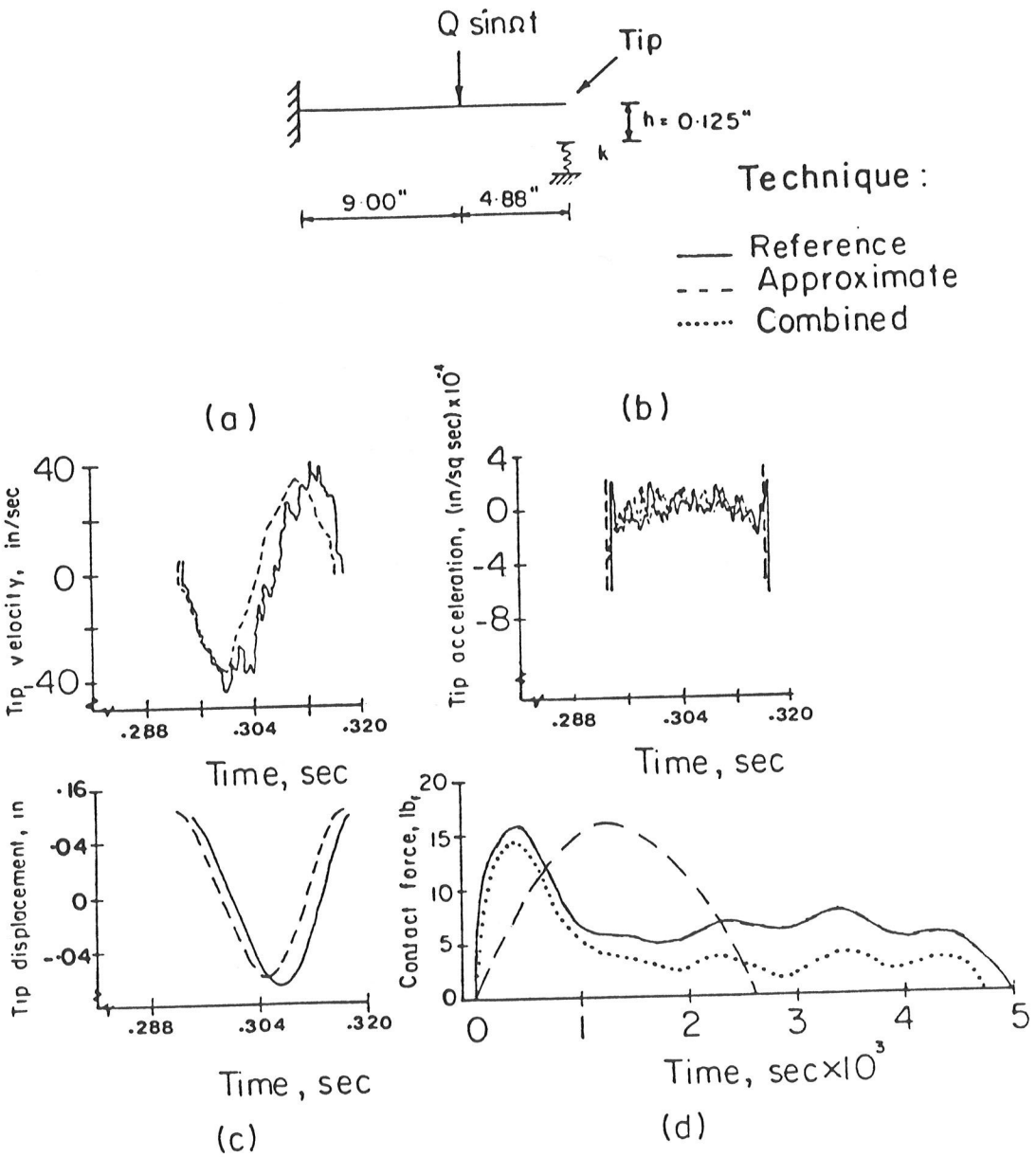

Figure 8. A comparison of different approaches for determining late (exemplified by the eleventh) contact details for the system of Figure 6 and 7.

```
RUN
GRAPHICS DEMONSTRATION - VERSION:82-07-26

YOU MAY RETRIEVE DATA FILES FROM
THE FOLLOWING MASS STORAGE DEVICES:
   F8 - FLOPPY DISK DRIVE
   T14 - LEFT CASSETTE DRIVE
   T15 - RIGHT CASSETTE DRIVE

ENTER FILE DEVICE
?
F8
ENTER FILE NAME ON FILE DEVICE - F8
?
FATHIB

FILE IS - FATHIB:F8
IF OK THEN USE <CONT-KEY> TO CONTINUE; OTHERWISE USE <STOP-KEY>

YOU MAY VIEW EITHER THE TIME HISTORY OF JUST
THE Y-DISPLACEMENT OF THE MOVING NODES <BRIEF> OR
ADDITIONAL PROPERTIES OF THE MOVING NODES
AS WELL AS THE DISPLACEMENTS <FULL>

SELECT EXTRA INFORMATION <0 - BRIEF, 1 - FULL>
?
1

YOU MAY VIEW EITHER VELOCITY AND ACCELERATION DATA(0)
OR BENDING MOMENT AND SHEAR STRESS DATA(1)

SELECT TYPE OF EXTRA INFORMATION <0 OR 1>
?
0

YOU MAY HAVE THE ANIMATION PROGRAM ERASE THE WHOLE
MOVING PORTION COMPLETELY BEFORE REDRAWING IT IN
THE NEW POSITION OR INTERLACE THE ERASING AND
REDRAWING FOR EACH LINK

SELECT ERASING TECHNIQUE <0 - INDEPEND., 1 - INTERLACE>
?
1
DO YOU WISH A LISTING OF INPUT? <0 - NO, 1 -YES>
?
0

YOU MAY VIEW EITHER THE WHOLE OBJECT
   (MACROSCOPIC VIEW) OR ONE EXPANDED
   DETAIL (MICROSCOPIC VIEW) OR CHOSE
   YOUR OWN VIEW (CUSTOM)

SELECT VIEW EXPANSION FACTOR <0 - MACRO, 1 - MICRO, 2 - CUSTOM>
?
1


EXCEPT FOR REPLIES TO PROMPTING MESSAGES
THE PROGRAM IS CONTROLLED BY THE FOLLOWING
FUNCTION KEYS -

<F-KEY 0> - TERMINATE THE PROGRAM
<F-KEY 1> - FREEZE THE ANIMATION AT THE CURRENT FRAME
<F-KEY 2> - CAUSE THE ANIMATION TO MOVE BACKWARDS
<F-KEY 3> - CAUSE THE ANIMATION TO MOVE FORWARDS
<F-KEY 4> - SINGLE STEP ANIMATION TO PREVIOUS FRAME
<F-KEY 5> - SINGLE STEP ANIMATION TO NEXT FRAME
<F-KEY 6> - RE-ARRANGE OR RE-INITIALIZE SCREEN FOR THE TIME HISTORIES
<F-KEY 7> - START POINTING TO SUCCESSIVE NODES FOR TIME HISTORY SELECTION
<F-KEY 8> - SELECT A NODE FOR TIME HISTORY
<F-KEY 9> - AS PER <F-KEY 8>, BUT STOP POINTING TO MORE NODES
<F-KEY 10> - RE-START THE ANIMATION AT THE MACRO/MICRO PROMPT
<F-KEY 11> - REQUEST ANOTHER SCREEN-FULL OF TIME HISTORIES
<F-KEY 12> - MAKE HARD COPY OF CURRENT GRAPHICS SCREEN
<F-KEY 13> - HELP TO EXPLAIN KEYS (I.E. THESE MESSAGES)
```

Figure 9. Illustrating the use of [illegible] computer package.

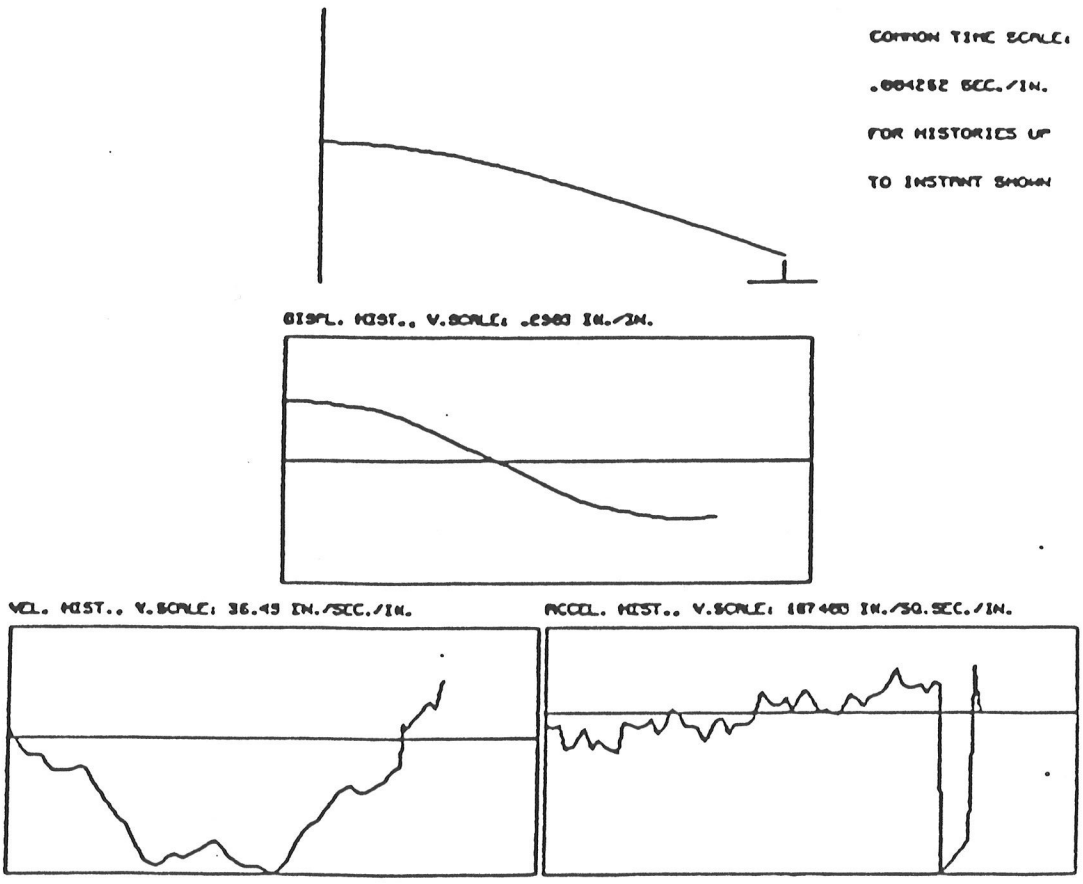

Figure 10. Typical "static" histories produced by using special programmable computer keys.

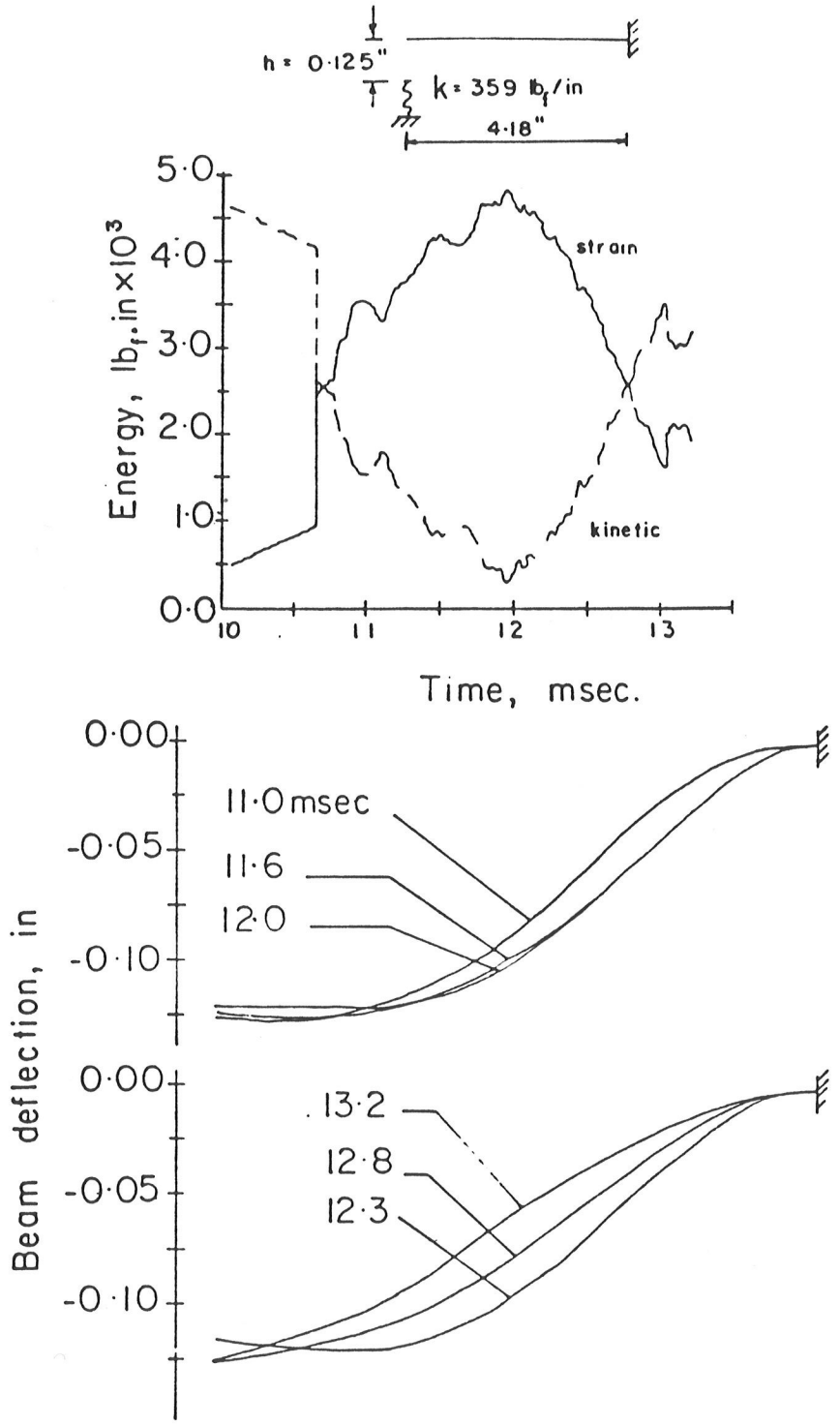

Figure 11. Showing (a) the unloaded vibroimpact system of reference [1]; (b) the beam's total kinetic and strain energies before and after the first impact at 10.67 msecs; and (c) beam shapes at different instants in the period during which chatter occurs. Material properties of the system are given in Table 1

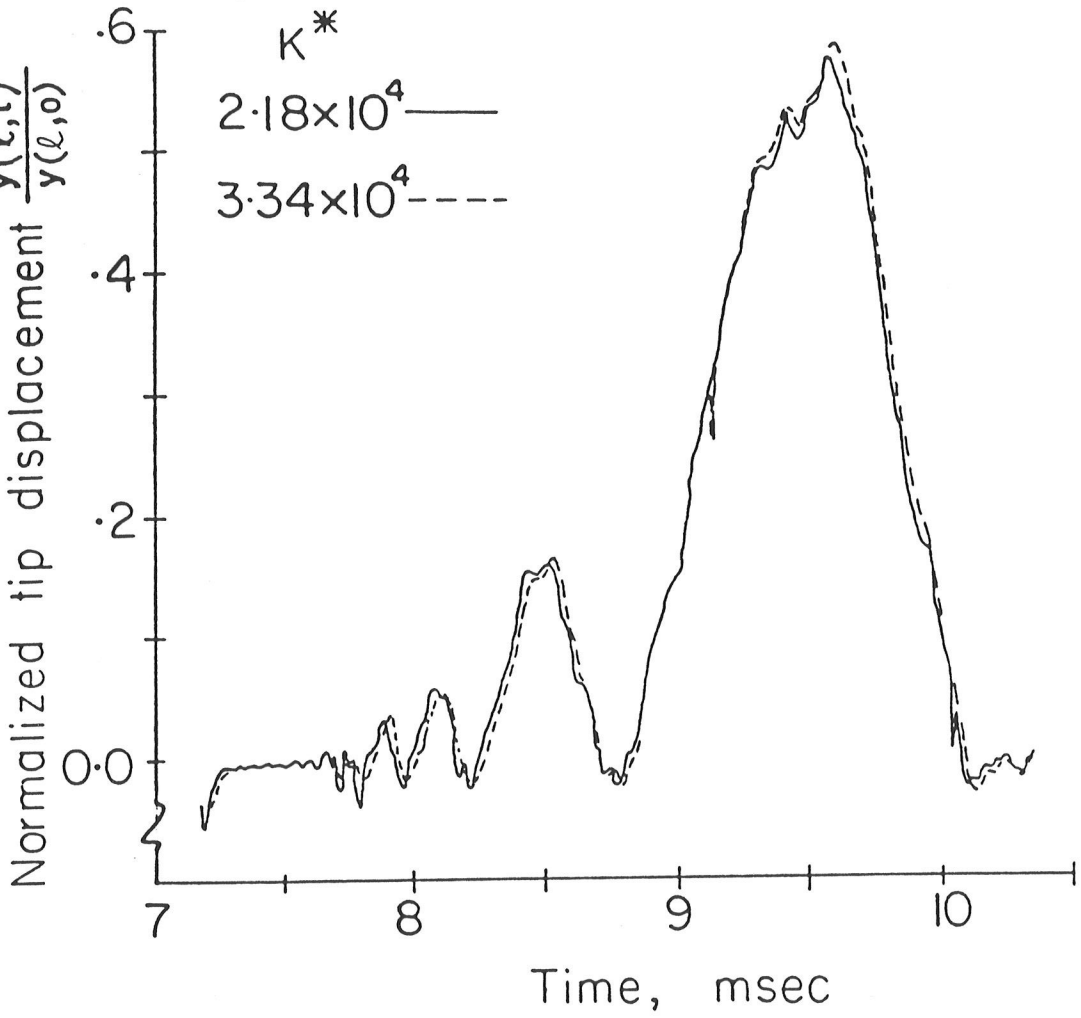

Figure 12. The effect of varying K* on the history of the normalized tip displacement of the vibroimpacting beam of reference [1] when h=-0.125in.

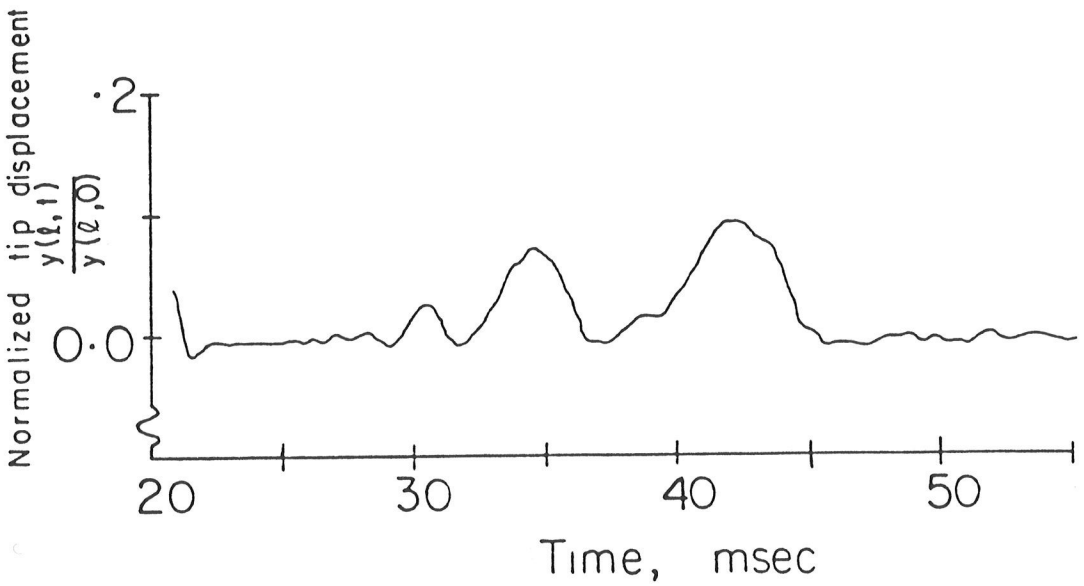

Figure 13. The effect of choosing a clearance magnitude, h, of -0.3 in. on the chatter amplitude associated with the system of reference [1] when $K^* = 2.18 \times 10^4$.

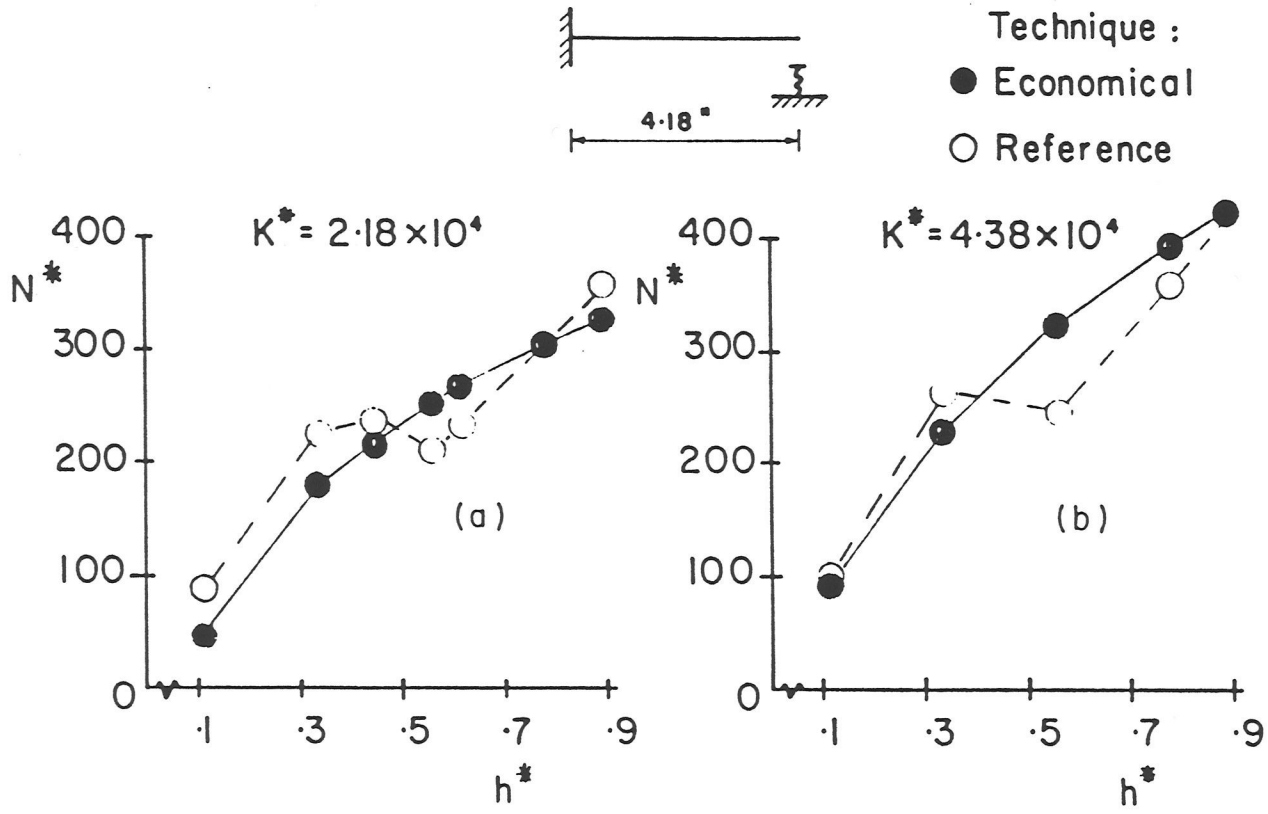

Figure 14. A comparison between reference and economically predicted N* corresponding to the two extreme values of 2.18×10^4 and 4.38×10^4 for K* and different h*.

Young's modulus	0.3×10^{8}	lb_f/in^2
Density	0.283	lb_m/in^3
Cross section AA'		
width	16.0	in
thickness	4.0	in
Damping	2 %	
Restrained point		
initial displacement	0.0	in
initial velocity	0.0	in/sec

(a)

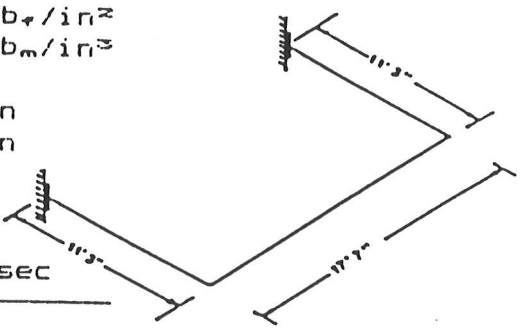

(b)

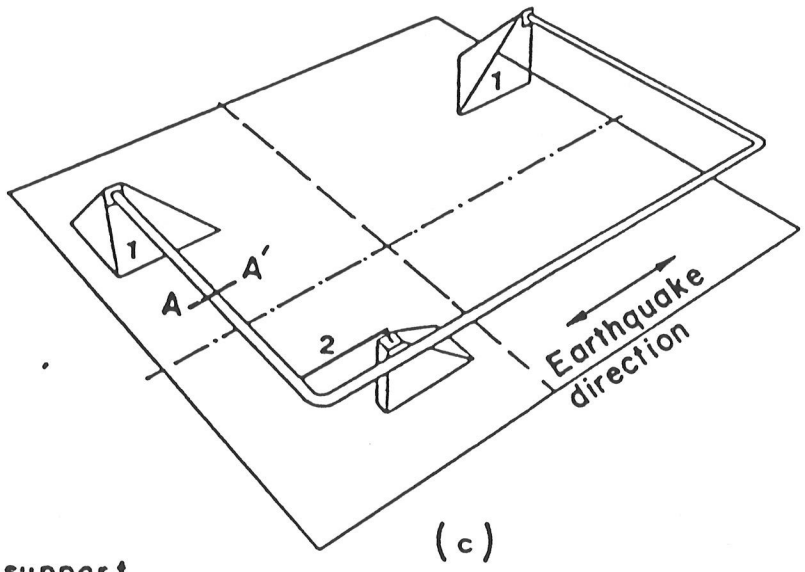

(c)

1 rigid support

2 restrainer

Figure 15. Showing (a) the material properties; (b) a schematic of a two-dimensional U-frame piping system; and (c) the restrainer location and direction of the exciting earthquake.

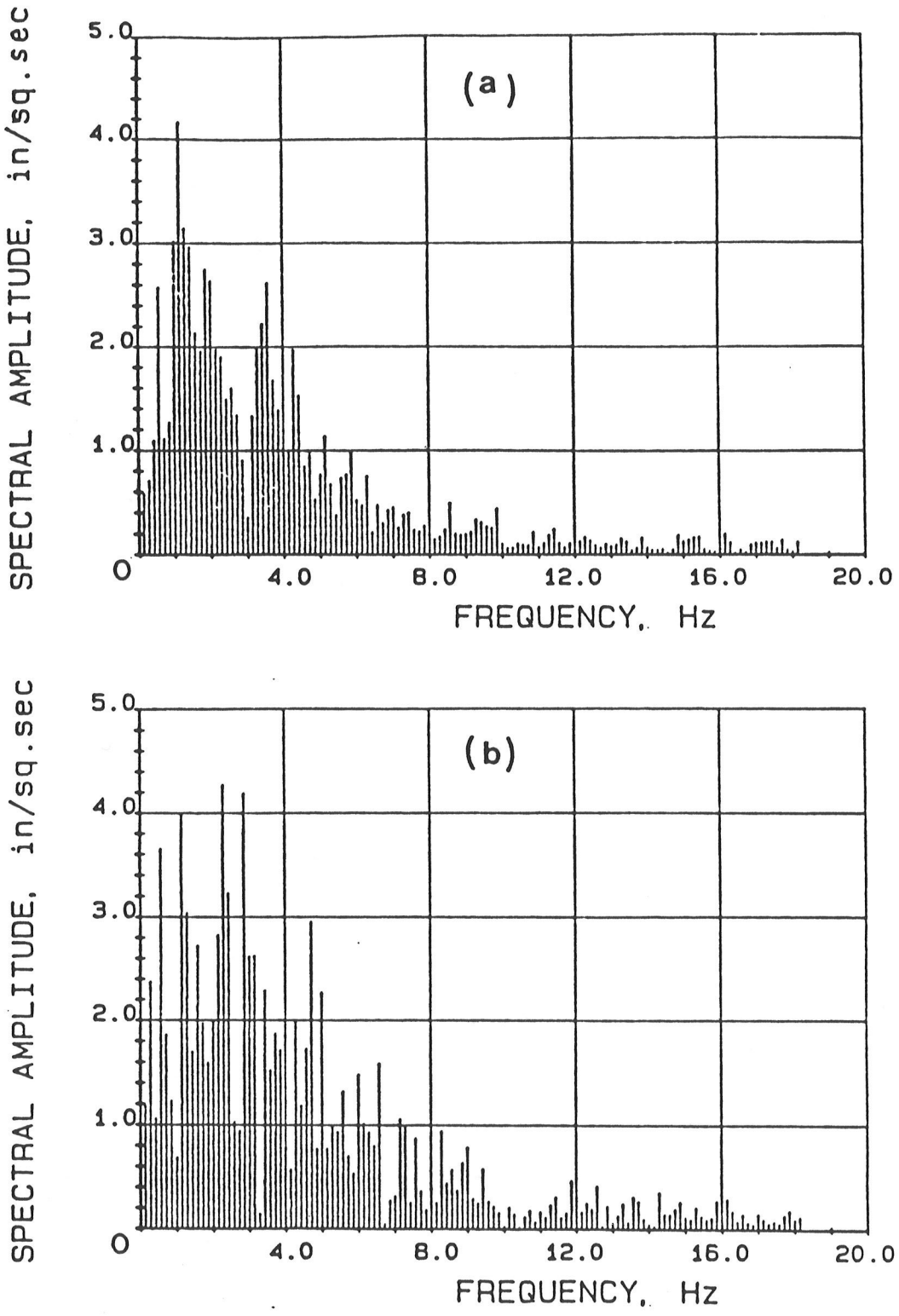

Figure 16. Acceleration spectra of the horizontal component of the (a) filtered and (b) unfiltered TAFT S69E earthquake.

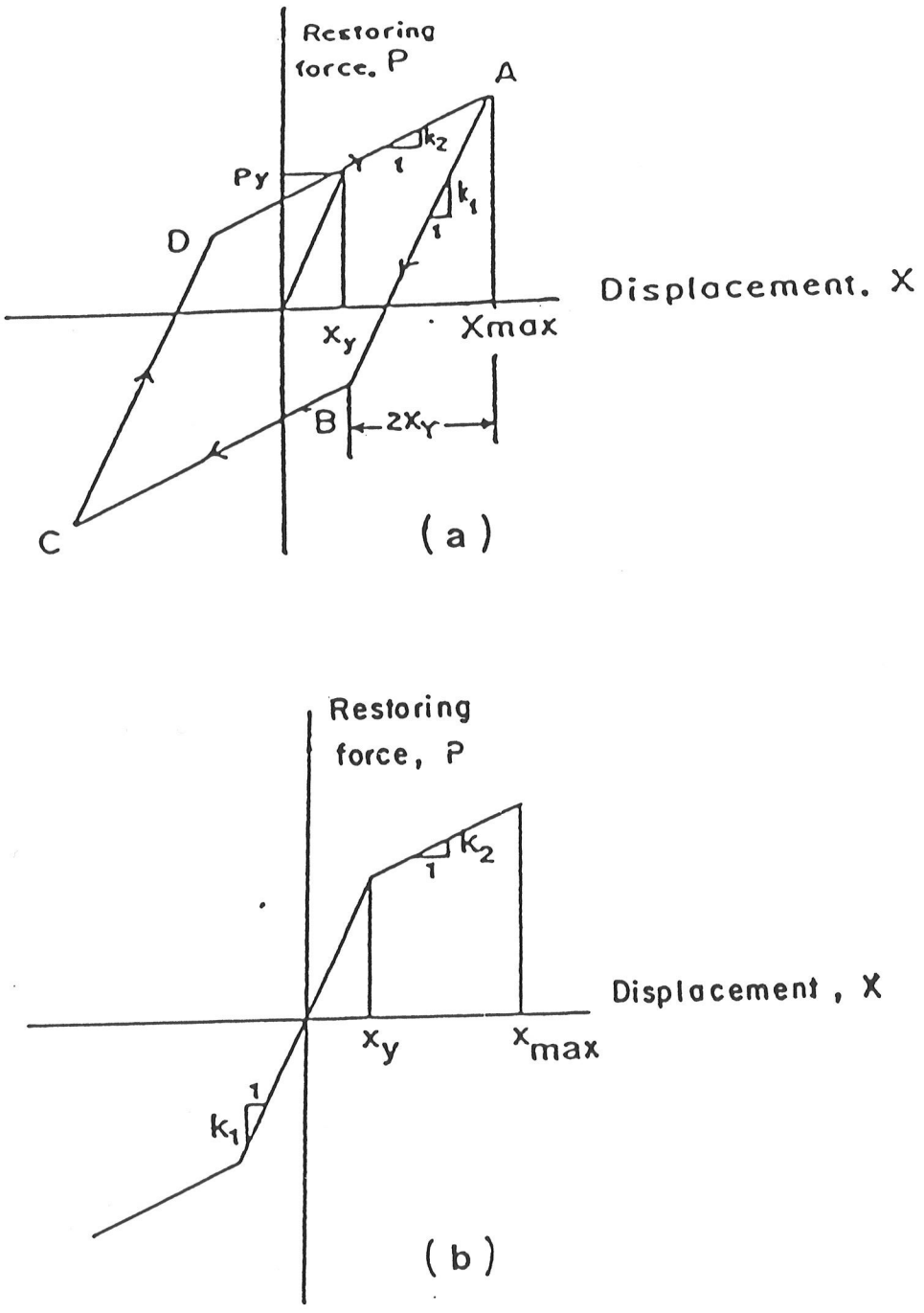

Figure 17. The load-displacement characteristics of (a) Masing and (b) hysteretic yielding material.

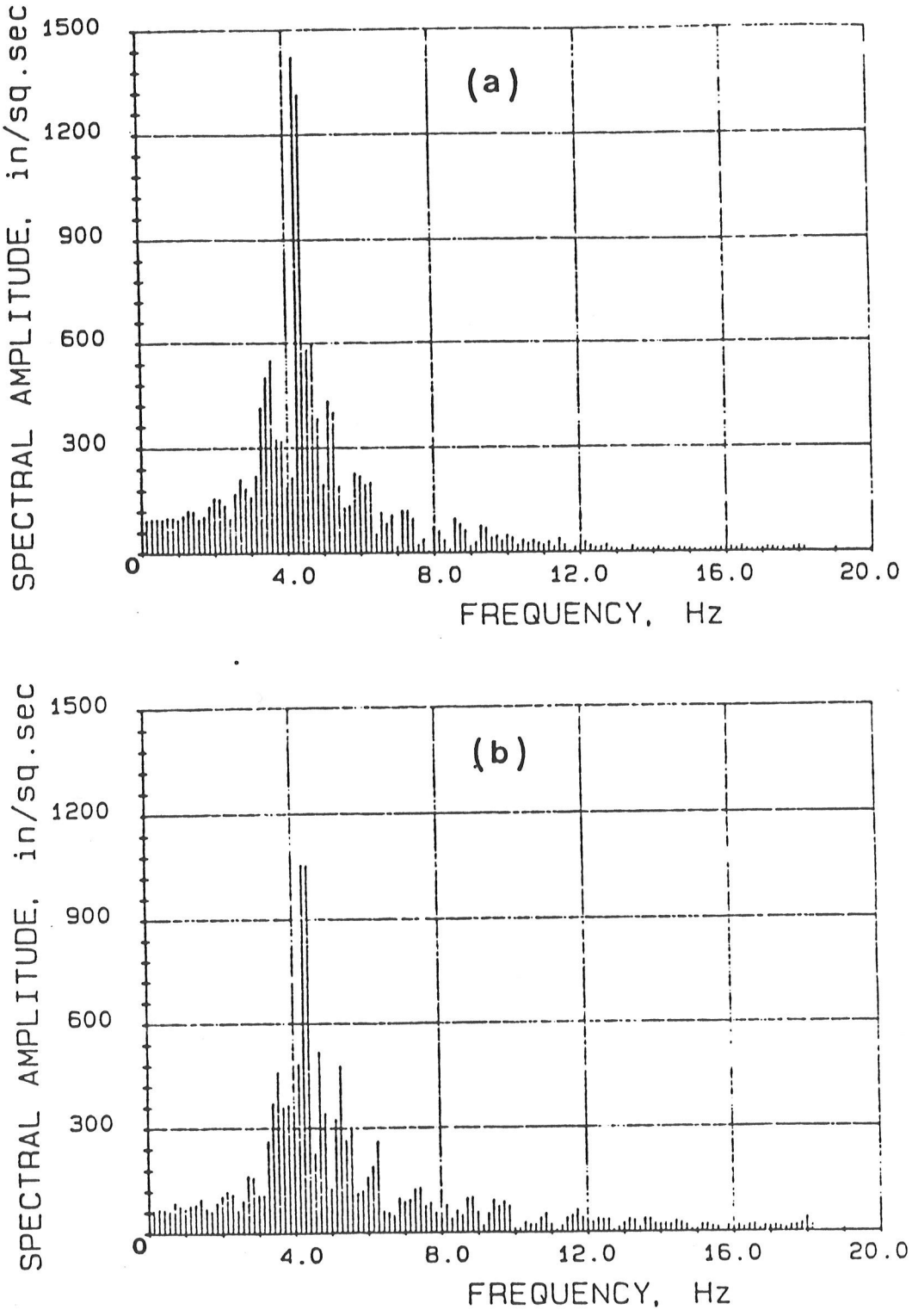

Figure 18. Acceleration spectra of the (a) unrestrained and (b) restrained piping system of Figure 15 excited by the filtered TAFT S69E earthquake. The restrainer consists of the yielding material with the general load-displacement characteristics given in Figure 17a. The restrainer's stiffnesses k_1 and k_2, are 3000 and 1500 lb_f/in, respectively. The yielding displacement, x_y, is equal to 0.11 inches.

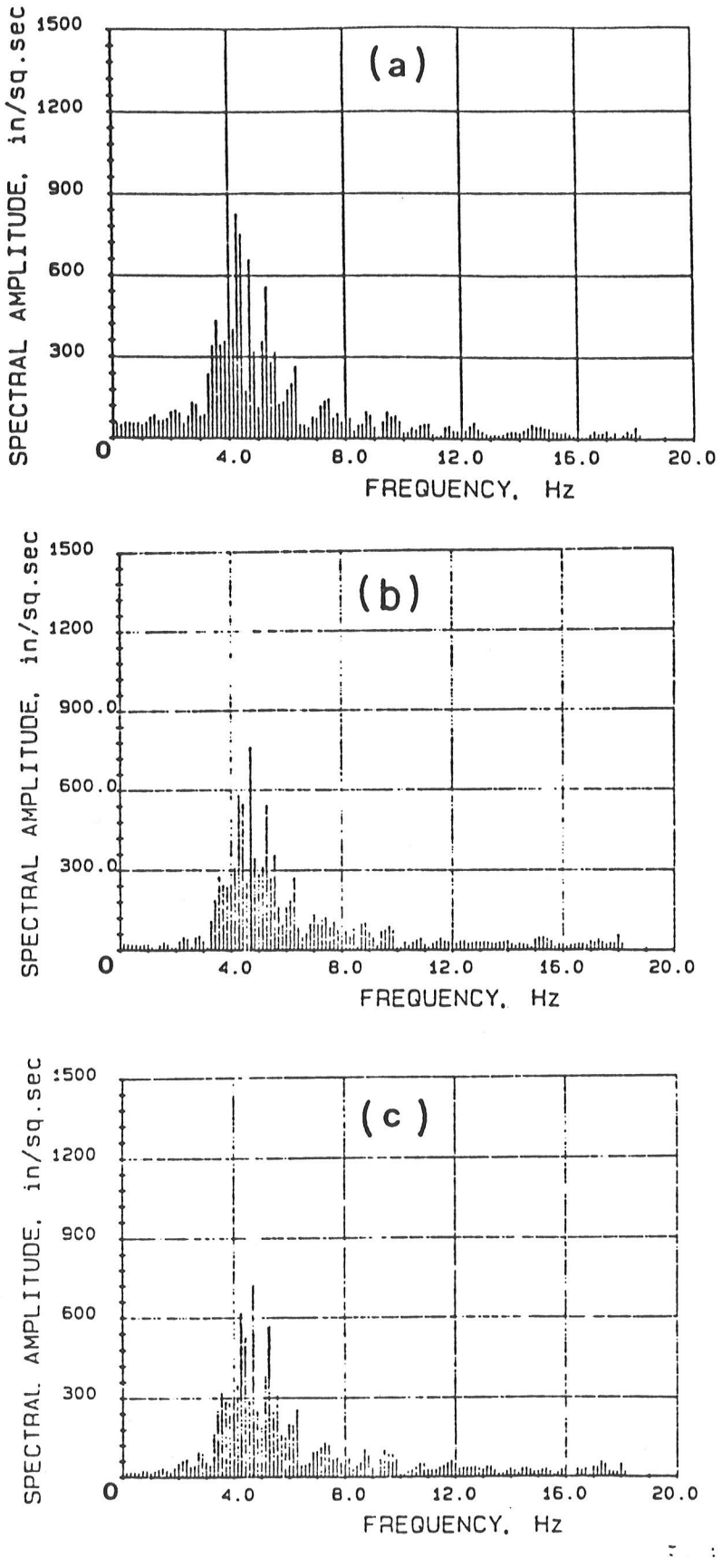

Figure 19. Acceleration spectra of the piping system of Figure 15 when excited by the filtered earthquake. The piping is restrained by a material with the load-displacement characteristics given in Figure 17a. The restrainer's stiffnesses K_1 and K_2, are 3000 and 1500 lb_f/in, respectively. The yielding displacement, x_y, is equal to (a) 1.0, (b) 5.0 and (c) 10 inches.

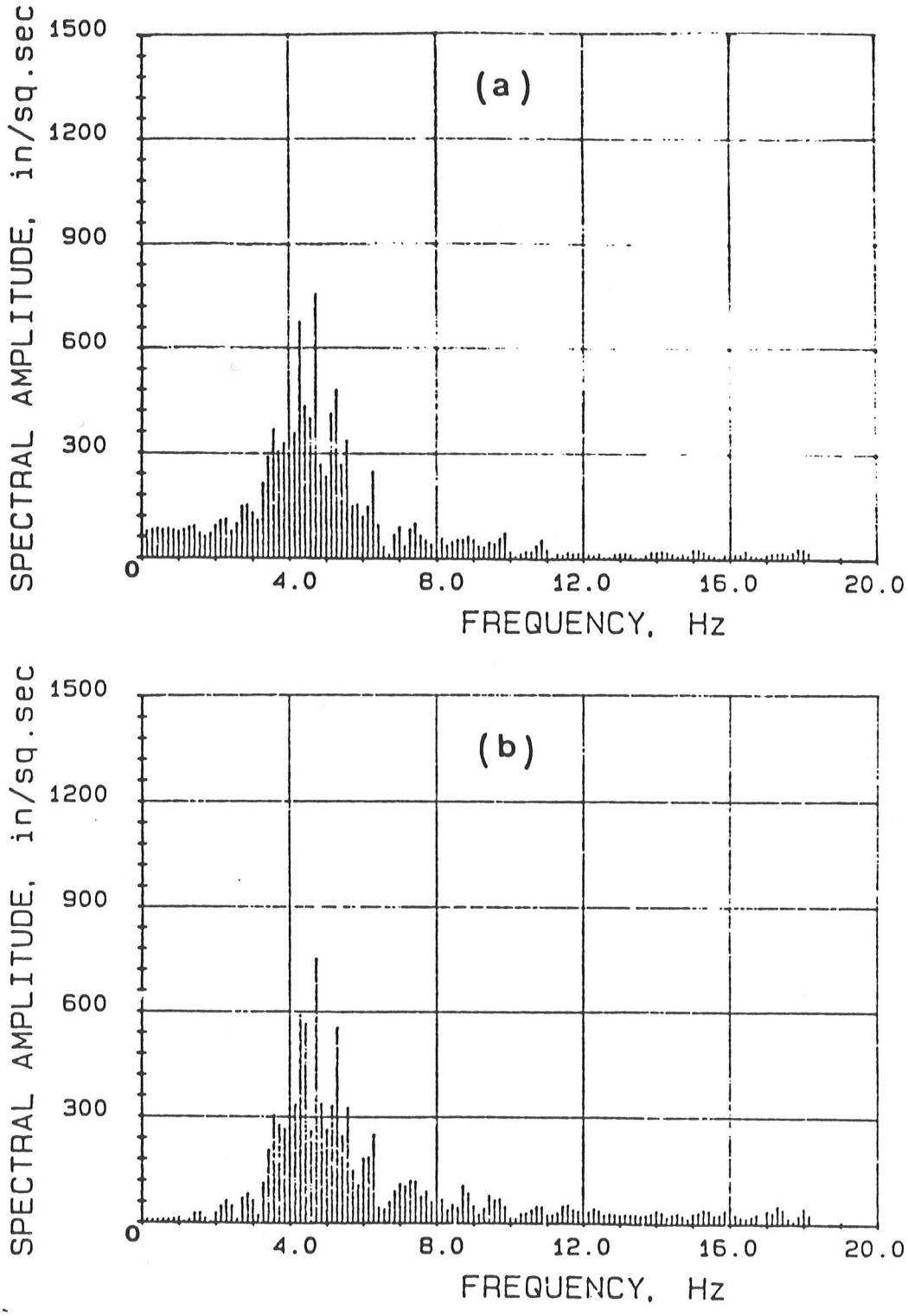

Figure 20. The effect of increasing x_y from (a) 5.0 to (b) 10 inches on the acceleration of the piping system of Figure 15 when excited by the filtered TAFT S69E earthquake. The restrainer consists of a hypothetical material with the general load-displacement characteristic of Figure 17b. Stiffness k_1 and k_2 is 3000 and 1500 lb_f/in, respectively.

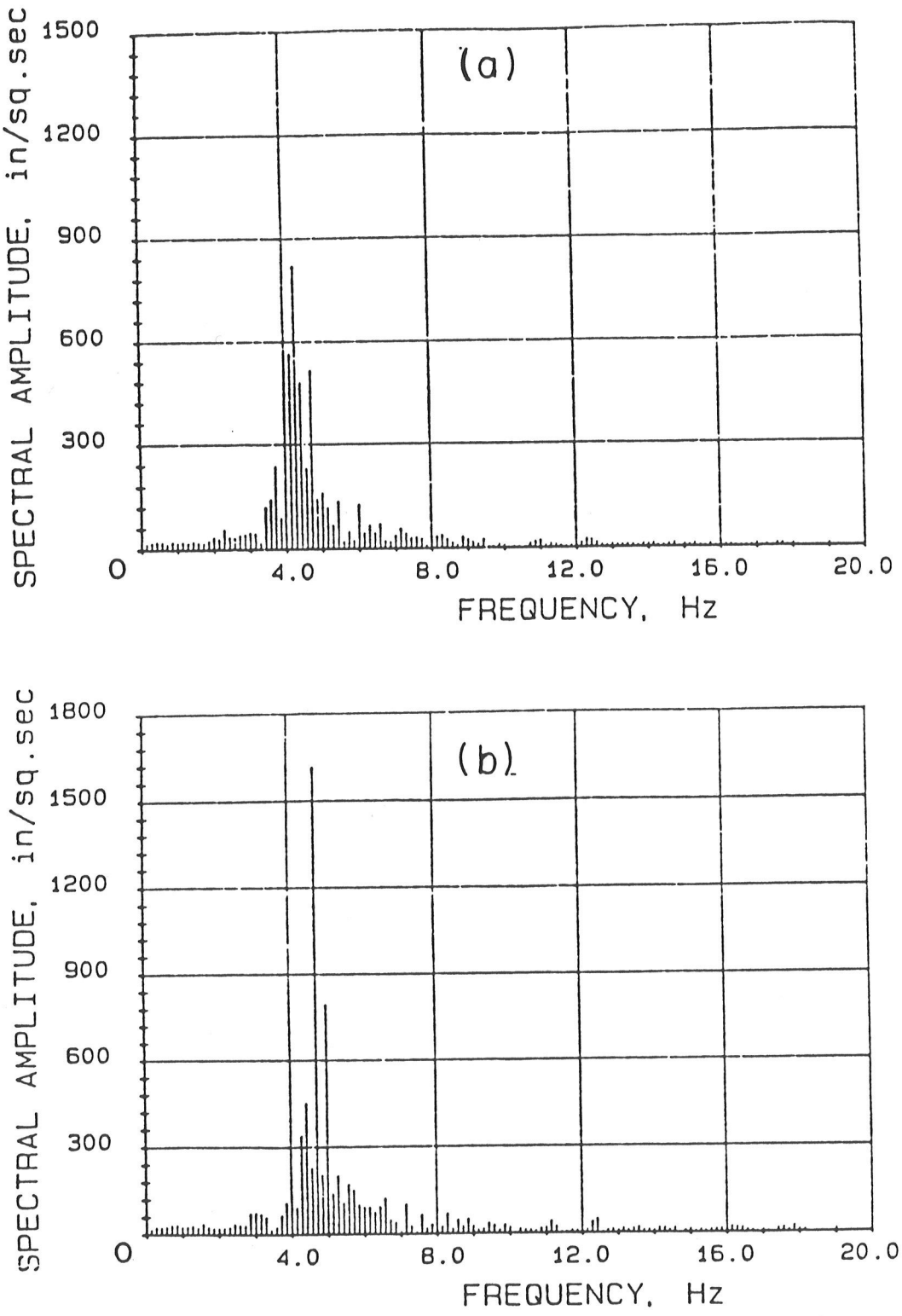

Figure 21. Acceleration spectra of the (a) unrestrained and (b) restrained system of Figure 15 when excited by the actual TAFT S69E earthquake. The restrainer consists of a true yielding material with the load-displacement characteristics given in Figure 17a. The k_1 and k_2, are 3000 and 1500 lb_f/in, respectively, and the yielding displacement, x_y, is equal to 5.0 inches.

	System properties appropriate to :			
	reference [1]		reference [2]	
Beam				
Young's modulus	0.178×10^{8}	lb_f/in^2	0.3×10^{8}	lb_f/in^2
Density	0.283	lb_m/in^3	0.286	lb_m/in^3
Cross section				
width	0.1	in	1.0	in
thickness	0.02	in	0.25	in
length	4.18	in	13.88	in
Stop stiffness	359	lb_f/in	10^5	lb_f/in
Damping ratio	0.0		0.003	
Nature of excitation	0.0	lbf	0.1 sin 265.14 t $\times \delta(x-9)$*	lbf

Table 1. Material and external load properties pertaining to the vibroimpact systems considered in reference [1] and [2].

* The δ is the dirac delta function.

Clearance, h (in)	Total kinetic or strain energy just before the first impact	
	Kinetic ($lb_f.in \times 10^{-3}$)	Strain ($lb_f.in \times 10^{-3}$)
- 0.1	4.7	3.0
- 0.2	3.8	1.2
- 0.3	2.8	2.2

Table 2. The effects of varying h on the total kinetic and strain energy just before the first impact of the vibroimpacting beam of reference [1].